Cellular and Molecular Life Sciences (2025) 82:220
https://doi.org/10.1007/s00018-025-05731-8

ORIGINAL ARTICLE

Tumor-associated macrophages contribute to cisplatin resistance via regulating Pol η-mediated translesion DNA synthesis in ovarian cancer

Bilash Chatterjee[1,2] · Mrinmoy Sarkar[1] · Debanjana Ghosh[1] · Sangita Mishra[1] · Subhankar Bose[1,2] · Md. Maqsood Ahamad Khan[3] · Senthil Kumar Ganesan[3] · Nabanita Chatterjee[4] · Amit Kumar Srivastava[1,2]

Received: 30 November 2024 / Revised: 18 April 2025 / Accepted: 29 April 2025

Abstract

Tumor-associated macrophages (TAMs) are known to be involved in the manifestation of aggressive and therapy-resistant phenotypes in solid tumors. Nevertheless, the effects of dynamic intervention by TAMs on the DNA damage response of cancer cells are largely unexplored. Herein, we report that TAMs modulate the DNA damage repair pathways of ovarian cancer cells in response to platinum-(Pt) based therapeutic regimen. We demonstrate that coculture of TAMs with cancer cells directly upregulate Pol η, along with RAD18 and REV1 of the Translesion DNA synthesis (TLS) pathway, while concurrently downregulating components of the high-fidelity nucleotide excision repair (NER) mechanism. Consequently, we observed a better survival probability, DNA repair capacity, and enrichment of stemness properties in ovarian cancer cells. DNA bulky adducts produced by cisplatin are resolved through differential activation NER and TLS pathways. However, we elucidated that TAMs provide favorable conditions for activating the error-prone TLS pathway for lesion bypass over damage resolution. Furthermore, cellular crosstalk in cocultured cancer cells stimulates the nuclear translocation and expression of RelA, which recruits Pol η by acting as a potent transcription factor. In fact, with pristimerin-mediated disruption of p65 (RelA) translocation, the cancer cells become more prone to DNA damage-induced cell death and compromised regenerative potential. In both in vitro cell cultures and in vivo mouse xenograft models, cocultured macrophages exhibited predominantly M2-like phenotype with prevalence in the invasive zone of xenograft tumor margins. Taken together, our investigation revealed multifaceted crosstalk-mediated regulation of DNA damage repair between TAMs and ovarian cancer cells.

Keywords Tumor-associated macrophage · Cisplatin resistance · Translesion DNA synthesis · DNA Polymerase eta · Cancerimmunotherapy

Introduction

The cellular landscape and spatiotemporal changes in tumor-infiltrating immune cells during different stages of ovarian cancer progression have significant and complex implications for the therapeutic response of cancer cells [1]. Pan-cancer evidence suggests that tumor-associated macrophages (TAMs) constitute the largest subpopulation of immune cells, accounting for more than 50%, and can actively modulate the tumor microenvironment toward an immunosuppressive niche [2, 3]. Although macrophages play a significant role in tissue repair, regeneration, angiogenesis, and wound healing in both cancer and noncancer tissues. However, there are no solid findings concerning whether TAMs can directly regulate the DNA damage response of cancer cells in response to chemotherapeutic drugs. The design of

✉ Amit Kumar Srivastava
amit@iicb.res.in

1 Cancer Biology and Inflammatory Disorder Division, CSIR-Indian Institute of Chemical Biology, Kolkata, West Bengal, India

2 Academy of Scientific and Innovative Research (AcSIR), Ghaziabad, Uttar Pradesh 201002, India

3 Structural Biology and Bioinformatics Division, CSIR-Indian Institute of Chemical Biology, Kolkata, West Bengal, India

4 Chittaranjan National Cancer Institute (CNCI), Kolkata, West Bengal, India

Published online: 29 May 2025

a patient-based therapeutic approach reveals the importance of characterizing the genetic, molecular, and cellular heterogeneity of the TME [4]. Therefore, more strategic research endeavors are needed to study the crosstalk between macrophages and cancerous and noncancerous immune and stromal cells to identify the molecular dynamics that determine chemotherapeutic failure or malignant recurrence.

The key aspects of cancer stem cell theory indicate that therapy resistance and cellular metastasis rely on a small population of cancer stem cells (CSCs) that typically reside in the tumor core region, which has compromised blood and lymphatic networks [5]. Although the existence of CSCs is controversial, they are now recognized as cells with efficient self-renewal, tumorigenic, and differentiation potential [6]. Pathways such as Notch, Wnt/β- Catenin, JAK- STAT, and Hedgehog tightly regulate CSC fate. In fact, dysregulated expression of these signaling pathways leads to CSC formation, contributing to transdifferentiation, tumor initiation, metastasis, chemoresistance, and tumor relapse [7]. This cell population is well-equipped to attract and recruit immunosuppressive MDSCs, Tregs, and TAMs, enabling their selective survival over other cells. The strategic location of TAMs correlates with the proximity of CSCs, the histological grade of solid tumors, and the number of CSCs [8]. Credible biomarkers for CSCs have been identified across different cancers [9]. Multiple cytokines secreted by M2-like TAMs, such as IL-17, PPARγ, TGFβ, and VEGF, are involved in maintaining the ovarian CSC niche and self-renewal capacity [10]. Conversely, CSCs promote infiltrated macrophages to skew towards an M2-like phenotype for pro-tumoral behavior [11]. Naturally, the tolerance of cancer cells to DNA damage is considered the primary factor responsible for the poor clinical response of chemotherapeutic drugs in many cases. Notably, chemotherapy is effective in the initial stages but fails to contain the disease as it advances into a more aggressive phenotype. UV- or platinum-based drug-induced DNA damage primarily involves the activation of the nucleotide excision repair (NER) pathway and the error-prone translesion DNA synthesis (TLS) pathway to some extent. NER surveillance proteins, such as XPC, efficiently recognize bulky DNA distortions, followed by the recruitment of the XPB/XPD helicase complex and the endonucleases XPG and XPF for coordinated action in resolving DNA lesions [12]. However, the TLS pathway may alleviate stalled replication or even minimize postreplicative DNA gaps [13]. Numerous reports have suggested that resistance to chemotherapy directly results from the local release of soluble factors that promote tumor growth, oncologic trogocytosis, and immune cell-driven remodeling of TME, ultimately expediting the acquisition of drug resistance [14].

Hence, our study focused on TAM-mediated chemotherapy tolerance in ovarian cancer cells to further understand how tumor-associated macrophages can regulate the DNA damage response by modulating multiple repair pathways on a conditional basis.

Materials and methods

Bioinformatics analysis

The gene expression profile of human high-grade serous ovarian cancer (HGSOC) was retrieved from the publicly available Gene Expression Omnibus (GEO) Database (https://www.ncbi.nlm.nih.gov/geo/query/acc.cgi?acc=GSE184880) GSE184880. (Total No = 6 samples, 3 malignant ovarian tumors and 3 nonmalignant ovarian samples) The dataset consisted of 10X Genomics-based single-cell landscapes of the HGSOC ecosystem, and the sequencing was performed via the GPL24676 Illumina NovaSeq 6000 platform [15]. The expression files generated from 10X Genomics in the form of features, barcodes, and matrices were downloaded from the GEO Database (https://www.ncbi.nlm.nih.gov/geo/). The extracted files were processed in "R"Studio (version 4.2.1; https://cran.r-project.org/bin/windows/base/old/4.2.1/) by using "Seurat package" (version 4.3.0;https://cran.rproject.org/web/packages/Seurat/index.html). The LogNormalize function was used to normalize the matrix files and obtain normalized counts. Furthermore, the FindVariableFeatures, ScaleData, RunPCA, and FindAllMarkers were utilized to determine the highly variable features, perform linear transformation, conduct principal component analysis (PCA), and detect differentially expressed genes (DEGs), respectively. For dimensionality reduction, the top 20 principal components were used for the t-distributed stochastic neighbor embedding (t-SNE). The Louvain modularity optimization algorithm was used at a resolution of 0.5 to identify different cell clusters [16]. Cell type annotation was performed based on known markers and the Human Proteome Atlas [17]. Candidate gene expression profiles across different ovarian cell types were visualized using FeaturePlot.

Protein–protein interaction and gene set enrichment analysis

The web-based server Metascape (https://metascape.org/gp/index.html#/main/step1) was used for pathway enrichment analysis, biological process, cellular distribution, and the associated involvement of transcription factors [18]. Furthermore, we carried out our analysis through the GeneMANIA webserver (https://genemania.org/search/homo-sapiens/) to explore coexpression, colocalization, physical interaction, and associated molecular function of

the shortlisted genes from the macrophage and cancer cell clusters independently [19].

Cell lines and cell culture

Ovarian cancer cell lines, including OV2008, OVCAR3, SKOV3, PA1, TR127, and ID8 were generously gifted by Dr. Qi-En Wang (The Ohio State University, Columbus, USA). The THP1 cell line was purchased from the National Centre for Cell Science (NCCS, Pune, India). OVCAR3, TR127, OV2008, and SKOV3 cells were cultured in RPMI 1640 (Gibco, USA) media supplemented with 10% FBS (Gibco, USA) and 1% antibiotic/antimycotic solution (Himedia). The PA1 and ID8 cell lines were cultured in DMEM (Gibco, USA) supplemented with 10% FBS and 1% antibiotic/antimycotic solution. All the cultured cells were maintained in a humidified incubator with 5% CO_2 at 37 °C. For in vitro experiments, four groups were established: (1) control, (2) cisplatin-treated, (3) cocultured cells, in which the ovarian cancer cells were cocultured with THP1 monocytes for 72 h, and (4) cocultured cells + cisplatin, in which, after 48 h of coculture, cisplatin (20 μM) was added and incubated for an additional 24 h.

Western blot

Western blot analysis was carried out using standard methods [20, 21], and all the primary and secondary antibodies were obtained from commercial sources. Briefly, trypsinized cells were lysed in RIPA buffer (GCC Biotech), followed by sonication and centrifugation. SDS−PAGE was performed for protein separation from cell lysate or nuclear extracts. After being transferred to a PVDF membrane, the membrane was blocked with 5% bovine serum albumin (BSA) in Tris-buffered saline containing 0.1% Tween® 20. HRP-conjugated anti-rabbit secondary antibody (Abcam) and enhanced chemiluminescence reagent (Takara) were used for protein visualization. The signals were detected via a ChemiDoc imaging system (Bio-Rad, USA).

The following antibodies and kits were used

XPC (Abcam-ab309129), RAD18 (CST-9040T), phospho-p44/42 MAPK (CST-4370T), phospho-γH2AX (CST-9718S), polymerase eta (Abcam-ab236450), p53 (CST-2527S), p65 (CST-8242S), HDAC1 (CST-34589S), phospho-chk2 (CST-2197T), cleaved-caspase3 (CST-9661T), GAPDH (CST-2118S), arginase 1 (CST-93668S), horseradish peroxidase (HRP)-anti-rabbit-IgG secondary antibody (Abcam-abcam-ab6721), goat anti-rabbit IgG H&L (Alexa Fluor 488; Abcam-ab150077). Anti-CD44 (FITC; MACS Miltenyi-130–113–341), anti-CD117 (PE; MACS Miltenyi-130–111–592), anti-CD206 (PE; BioLegend-141703), anti-CD163 (FITC; BioLegend-111803), anti-mouse CD44 (FITC; BioLegend-156007), anti-mouse CD133 (PE; BioLegend-141203), and anti-mouse CD163 (PE; BioLegend-111803) antibodies were used. The chemicals and kits used were the Human Cytokine Array Kit (R&D Systems-ARY005B), pristimerin (Sigma-P0020), Hoechst 33342 (Invitrogen-H1399), and cisplatin (Sigma-P4394).

Transfection and molecular cloning

Human *POLH* shRNA (Cat no: EcoliVB200131-1181xqd; product detail: pPB[shRNA]-Puro U6 > hPOLH[shRNA#1]) was purchased from Vector Builder, USA. Lipofectamine™ 2000 (Life Technologies) was used to transfect the siRNAs and shRNAs into the ovarian cancer cells. To establish stable *POLH*-deficient cell lines, the shPOLH plasmid was transfected into OVCAR3 cells. Puromycin (2 mg/mL) was used to select stably transfected cell clones.

Transwell migration assay

Cell migratory ability was analyzed via a transwell insert (8-μm pore size) system in a 6-well format. Cells in incomplete media were seeded in the upper chamber of the insert. RPMI complete media (10% FBS) was added to the bottom chamber of the plate, which was subsequently incubated for 16 h at 37 °C and 5% CO2 in a humidified incubator. The migrated cells were fixed in 100% methanol (for 20 min) and stained with 0.5 % (w/v) of methylene blue. The number of migrated cells was counted under an inverted microscope for each group (6 random fields/well).

Real-time PCR

Total RNA was extracted via RNA iso plus (TAKARA). The extracted RNA was reverse transcribed using the PrimeScript™ RT reagent Kit. Quantitative real-time PCR was performed via iTAq Universal SYBR Green Supermix (Bio-Rad). *GAPDH* served as a reference gene, and the $2^{-\Delta\Delta Ct}$ method was used to quantify the fold change across the groups. The sequences of the primers are provided in Table 1.

Cytokine array

A membrane-based cytokine array was performed with the conditioned media from the groups. The Proteome Profiler Array Kit (Human Cytokine Array Kit; R&D Systems-ARY005B) was used for this purpose and was performed in accordance with the manufacturer's protocol.

Flow cytometry

For the analysis of enrichment of surface markers, all the single-cell suspensions from the groups (in 2% BSA

Table 1 The primer sequences used for Real-time PCR

Real time quantitative PCR primers-	
GAPDH	Forward – 5'-GAAGGTGAAGGTCGGAGT-3'
	Reverse – 5'-GAAGATGGTGATGGGATTTC-3'
POLH	Forward – 5'-GCGGTGACAGCCACTAAG-3'
	Reverse – 5'-GTAATGAGGGCTTGGATGG-3'
REV1	Forward – 5'-TGGCAGTATTACCAGAATAAAATCC-3'
	Reverse – 5'-TCTGGATTCTCCCACAATGA-3'
RAD18	Forward – 5'-CAGCTGTTTATCACGCGAAG-3'
	Reverse – 5'-TTAAATCACGATCAGAGCAAA-3'
XPC	Forward – 5'-GCCGAGACCTTGAGACCATA-3'
	Reverse – 5'-AGGCTGGTCCATGTGTTTTG-3'
XPA	Forward – 5'-GACACAGGAGGAGGCTTCATT-3'
	Reverse – 5'-TCGCATATTACATAATCAAATTCCATA-3'
XPB	Forward – 5'-ACTGGATGGAGCTGCAGAAT-3'
	Reverse – 5'-GGAGACATAGGGCACCAGAC-3'
XPG	Forward – 5'-CCAAGCGCAGAAGAACATTA-3'
	Reverse – 5'-TTAAGCAAGCCTTTGAGTTGG-3'
XPD	Forward – 5'-TTGAGACCCGGGAGGATATT-3'
	Reverse – 5'-ATGCCATCAGGGACCACA-3'
CHIP primers-	
Primer 1	Forward – 5'-AAGAACGAAGCTGGTGTTGG-3'
	Reverse – 5'-GCTTCTGTGCACTCTTGTCC-3'
Primer 2	Forward – 5'-GCACAGAAGCGAGGAAAGG-3'
	Reverse – 5'- CAAATCGCCGCCTTCTCTAC-3'

solution) were stained with fluorescent tagged antibodies and incubated for 30 min. The antibodies used were anti-human CD44 (FITC), CD117 (PE), CD206 (PE), and CD163 (FITC), anti-mouse CD133 (PE), and CD44 (FITC). For the live/dead assay, propidium iodide (1 mg/ml)-positive dead cells were analyzed. In contrast, phospho-γH2AX-positive cells were analyzed by anti-phospho-γH2AX (PE) staining of 70% ethanol-fixed cells and incubated for 30 min at 4 °C in the dark. All the data were acquired on a BD LSRFortessa™ flow cytometer and analyzed with FlowJO software version 8.

Comet assay

Around 30000 cells were seeded in a 12-well plate for each of the four groups. After the incubation, cells were washed with PBS and trypsinized to obtain a cell pellet. The further downstream process for the comet assay was performed as described by Wani et al. [22]. Images were taken with a fluorescence microscope, and tail length was analyzed via ImageJ software.

NF-κB blockade via pristimerin

Pristimerin was used to inhibit the activation of p65 in cancer cells. Pristimerin was diluted in PBS and added to the corresponding groups (2 μM for 24 h).

Bone marrow-derived macrophage (BMDM) isolation and coculture

BMDMs were generated from 6–8-week-old C57BL/6 mice as described by Guc et al. [23]. Notably, conditioned media from the mouse ovarian cancer cell line (ID8) was supplemented (1:1) with fresh complete DMEM to culture the isolated cells for 7 days, after which the M2 macrophage population was characterized via flow cytometry. For immunocytochemistry of the ID8 cell line, in the cocultured group, the ID8 cell line was cocultured with BMDMs for 72 h, whereas in the cocultured + cisplatin treated group, the ID8 cells were cocultured with BMDMs for 72 h, and cisplatin treatment (20 μM) was applied for 24 h after 48 h of coculture.

CSC spheroid generation and culture

Ovarian cancer cells were seeded (0.2×10^6 cells/well) in a six-well ultralow attachment plate (Corning, USA). DMEM/F12 + GlutaMAX™ (1X) media (Gibco, USA) supplemented with 20% Knockout™ SR (Gibco, USA), bFGF (20 ng/ml) (Gibco, USA), and EGF (20 ng/ml) (Gibco, USA) was used. The seeded cells were cultured at 37 °C with 5% CO_2 in a humidified incubator for 3–4 days to develop spheroids. For cocultured spheroids, ovarian cancer cells and THP1 cells were seeded at a ratio of 3:1, while 0.2×10^6 cells/well was the seeding density.

Live spheroid staining with Hoechst 33342 dye

The CSC spheroids were washed in PBS and then resuspended in fresh PBS. Hoechst 33342 was used to stain the spheroids for 15–20 min. The efficiency of the staining was checked periodically. All images were taken with fluorescence microscope.

Immunocytochemistry

Cells were seeded (0.1×10^6 cells/well) on a sterilized coverslip for each group in a six-well plate. For the cocultured groups, cancer cells and THP1 cells were seeded together at a 2:1 ratio. All the groups were incubated for 72 h at 37 °C in a humidified incubator with 5% CO_2. At 48 h of coculture, the respective groups were treated with 20 µM cisplatin for an additional 24 h. The coverslips were then carefully washed with PBS (3 times). Subsequently, the cells were fixed with 4% PFA for 15 min, followed by incubation at room temperature with Triton X-100 (0.2% v/v in PBS) for 10 min. After subsequent washes with PBS, the cells were blocked with 2% BSA solution (in PBS) for 1 h at room temperature, followed by incubation with primary antibodies at appropriate dilutions overnight at 4 °C. The following day, cells were incubated for 2 h with Alexa Fluor 488-conjugated secondary antibody, after PBS wash (2 times, 5 min each). Nuclei were counterstained with Hoechst 333342 for 5 min, and subsequently, the coverslip was mounted on a microscopic slide with Fluoromount™ aqueous mounting medium (Sigma Aldrich-F4680). Images were acquired using high-resolution confocal microscopy.

Wound healing assay

Ovarian cancer cells were seeded in 12-well plates. For coculture, THP1 cells were seeded in the upper chamber of a transwell insert system (0.4 µm), and ovarian cancer cells were seeded in the lower chamber. Each well of each group was then scraped with a 10 µl pipette tip, then was incubated in a humidified incubator for 24 h in the incomplete medium. Wound healing was calculated according to the percentage change in wound size over 24 h.

THP1 differentiation

THP1 monocytes were treated with 100 nM PMA (initially dissolved in DMSO and further diluted with complete RPMI media) for 48 h to obtain differentiated M0 macrophages. The media was changed after 48 h, and differentiated macrophages were either cultured alone or cocultured with ovarian cancer cell lines/conditioned media for further downstream experiments.

Cell cycle analysis

Cells from the different groups were trypsinized, collected in 1.5 ml microcentrifuge tubes, subsequently prefixed with 70% ethanol, and incubated at 4 °C for 24 h. The next day, after the ethanol was discarded and the cells were washed in PBS twice, the cells were again resuspended in 300 µl of PBS for each group. 2 µl of RNase A (10 mg/ml) was added, and the mixture was incubated for 30 min at room temperature. Then, 5 µl of propidium iodide solution (1 mg/ml) was added to each tube. The data were acquired on a BD LSRFortessaTM flow cytometer and analyzed with FlowJo software version 8.

CHIP qPCR analysis

The ChIP assay was performed via the SimpleCHIP® Plus Enzymatic Chromatin IP Kit (Magnetic Beads) (CST −9005). The immunoprecipitated and purified DNA was analyzed via real-time quantitative PCR with iTAq Universal SYBR Green Supermix (Bio-Rad). The primers used for ChIP−qPCR are listed in Table 1.

In vivo studies

All the animal studies were performed in accordance with the institutional guidelines of CSIR-IICB (Animal ethics approval- IICB/AEC/Meeting/Sep/2023/1). The human xenograft tumor model was developed using nude mice (6–8 weeks old). The animals were purchased from Tata Memorial Centre, Mumbai, India and were kept in the institutional animal facility. OVCAR3 cells (3×10^6) were dissolved in RPMI media and Matrigel (Corning, USA) in equal volumes and inoculated subcutaneously into the flanks of 10 mice. In contrast, OVCAR3 and THP1 (2:1) cells were coinjected into another 10 mice. Each of these two sets was further subdivided into

cisplatin-treated and untreated subgroups, altogether forming four groups, namely control group, cisplatin-treated group, OVCAR3(shcontrol) + THP1 coinjected group, and OVCAR3(shcontrol) + THP1 coinjected + cisplatin group. Similar experimental groups were generated with OVCAR3 (shPOLH) and THP-1 cell lines. Two weeks after cell inoculation, tumor-bearing mice were randomized and divided (blinded) into four groups (5 mice for each group), and four doses of cisplatin (5 mg/kg body weight) were administered intraperitoneally, with an interval of 2 days, to the 'cisplatin-treated' and 'coinjected + cisplatin-treated' groups. The tumor volume was monitored periodically via a digital Vernier caliper; accordingly, the tumor volume was calculated with the formula $(l \times b^2) \times {}^{1}/_{2}$, where l is the longest diameter and b is the shortest diameter of the tumor. At the end of the experiments, all the mice were sacrificed, and the tumors and inguinal lymph nodes were isolated and weighed. For cytokine analysis in peripheral blood, mouse blood samples were collected via retro-orbital puncture into appropriate collection tubes.

.

Immunofluorescence, immunohistochemistry, and histology (H&E) staining

For immunohistochemical staining, an immunohistochemistry (IHC) kit (Abcam-ab64261) was used, and the downstream process with the OCT-embedded cryosections of the tissues was performed as directed in the manufacturer's protocol. All the sections were counterstained with hematoxylin, the slides were visualized, and pictures were taken under an inverted light microscope (Olympus, Tokyo, Japan). The antibodies used were phospho-γH2AX (CST) and cleaved caspase-3 (CST).

4% paraformaldehyde-fixed tissue sections were subjected to immunofluorescence staining. The antigen retrieval process was carried out following a standardized protocol [24]. The sections were blocked with 2% BSA solution in PBS containing 0.3% Triton X-100 (v/v) for 60 min. The sections were then incubated with primary antibodies overnight at 4 °C using recommended concentrations for individual antibodies. The next day, the tissue sections were washed in PBS (3 times, 5 min each) and incubated with an Alexa Fluor 488-conjugated anti-rabbit secondary antibody for 3 h at room temperature (dilution 1:400). Nuclei were counterstained with DAPI, and the tissue sections were mounted with Fluoromount™ aqueous mounting medium (Sigma Aldrich). The fluorescence stained images were captured using a fluorescence microscope (Bio-Rad). The antibodies used were phospho-γH2AX, Ki67, Pol η, p65, Arginase 1, and CD206.

For hematoxylin & eosin (H&E) staining, the tissues were gradually rehydrated through graded ethanol solutions in distilled water, followed by staining with hematoxylin. The samples were washed in running tap water for several minutes to wash off excess stain and achieve bluing. Next, the tissues were dehydrated with 70% ethanol and stained with eosin solution. Eventually, the tissues were gradually dehydrated through graded ethanol solutions, mounted with DPX, and observed under an inverted microscope.

Clinical sample processing

Patient sample-based experiments were carried out at Chittaranjan National Cancer Institute, Kolkata, India. (human ethics approval-CNCI-IEC-40104). Informed consent was obtained from all the subjects. The ovarian tissues were collected aseptically, and washed with PBS 2–3 times. Each patient sample was cut into two pieces. One set was fixed in 4% paraformaldehyde for further use in an immunofluorescence-based staining procedure, and the other set was immediately homogenized into a single-cell suspension via collagenase IV and passed through a cell strainer (40 µm). The homogenized tissue-derived cell suspension was used for flow cytometric analysis.

Statistical analysis

All the statistical analyses and graph generation were performed with GraphPad Prism version 8.0 (GraphPad Software, USA). The experimental data are presented as mean ± standard deviation (SD). The Brown-Forsythe and Welch's ANOVA test was performed assuming there is variance inhomogeneity. Accordingly, for multiple groups, Games-Howell's multiple comparisons test was performed to test the significance after the variance inhomogeneity test; one-way ANOVA followed by Tukey's post hoc test was performed otherwise. For experiments with two groups, unpaired two-tailed student's-*t*-test was performed. The level of significance is set as * $= p < 0.05$, ** $= p < 0.01$, *** $= p < 0.001$, and **** $= p < 0.0001$.

Results

Coculture of cancer cells with TAMs increases Pol η expression, thus contributing to DNA lesion bypass and promoting cancer stemness

The DNA polymerases involved in TLS are low-fidelity enzymes lacking 3′−5′ proofreading activity. These proteins include the Y-family polymerases: polymerase eta (η), iota (ι), kappa (κ), and REV1, among others. Strong evidence from kinetic studies indicates that Pol

η possesses the highest catalytic efficiency for bypassing cisplatin adducts among the Y-family polymerases. Increased expression of Pol η has been clinically associated with shorter survival in patients [25, 26]. Consequently, the correlation of Pol η expression across normal, tumor, and metastatic samples was gathered from TNMplot.com (Supplementary Fig. S1A) [27], while cancer stage-wise depictions and differential gene expression levels between normal and tumor tissues in ovarian cancer are represented by violin plots and box plots, respectively, from the Gepia2 database (Supplementary Fig. S1B, C) [28]. Pan-cancer heatmap analysis data from the TNMplot database also showed greater expression of Pol η in tumor tissue compared to normal tissue (Supplementary Fig. S1D). Therefore, this study primarily focuses on Pol η as an indicator of TLS activity. Intriguingly, Pol η expression was found to be elevated under coculture conditions, even without cisplatin treatment, compared to the control group, both at protein and mRNA levels. Additionally, other TLS-related genes, such as REV1 and RAD18, were also upregulated (Fig. 1A, B, C). In a DNA repair kinetics study (Fig. 1A), proteins from lanes 1–4 were extracted after cisplatin treatment (20 μM for 24 h); lanes 5 and 6 were collected 3 h after media change, while lanes 7 and 8 were extracted 6 h post-media change following cisplatin treatment. The results suggested that TAMs in the coculture setup not only elevated the Pol η levels in cancer cells but also facilitated quicker resolution of DNA damage. Next, we analyzed the enrichment of cancer stem-like cell subpopulations among the groups. Given that Pol η expression is directly correlated with enhanced stemness properties [29], we created a Pol η-deficient stable cell line (Supplementary Fig. S1E) from OVCAR3 to examine the effects of stem cell enrichment in both cocultured OVCAR3 shControl and OVCAR3 shPOLH (Pol η-deficient) cells. The enrichment of stem-like cells was significantly greater in the cocultured OVCAR3 shControl group and this effect was further enhanced by cisplatin treatment, compared to the untreated control and cisplatin-only groups. Surprisingly, no significant enrichment was observed in cocultured OVCAR3 shPOLH cells (Fig. 1D, E). The ID8 ovarian cancer cell line, cocultured with BMDMs, also confirmed the increase in Pol η expression (Supplementary Fig. S1F). As anticipated, through immunocytochemistry and flow cytometry analysis, we observed a better enrichment of stem-like ID8 cells in the coculture conditions (Supplementary Fig. S2A, B). Similarly, the enrichment analysis of other human ovarian cancer cell lines, including PA1, SKOV3, and TR127 (cisplatin-resistant cell line), mirrored the findings in OVCAR3 (Supplementary Fig. S3A, B, C). Since TR127 is a cisplatin-resistant cell line, the level of stemness enrichment did not significantly differ with or without cisplatin treatment (Supplementary Fig. S3B). The average diameter of spheroids formed from cocultured cancer cells was larger than that of the control, and spheroid shrinkage in response to cisplatin was consistently less in the cocultured spheroids. This indicates an enhanced chemoresistance trait in the cocultured spheroid group, as seen in both brightfield microscopy images and Hoechst-stained live cell images observed under a fluorescence microscope (Supplementary Fig. S3D, E) (Supplementary Fig. S4A, B).

The enrichment of stem-like properties significantly impacts the migratory potential of ovarian cancer cells. To investigate this, we performed transwell migration and scratch assays across multiple cell lines. We observed a consistent increase in the migratory potential of the cisplatin-treated cancer cells, which was even more pronounced under cocultured conditions and further amplified in the cisplatin-treated cocultured cells (Fig. 1F, Supplementary Fig. S4C, D). A similar trend was noted for wound healing ability (Supplementary Fig. S5A, B). Additionally, with heightened Pol η expression in cocultured cancer cells, the level of DNA damage following cisplatin treatment was significantly lower compared to untreated cancer cells (Fig. 1B). This was validated by immunocytochemistry analysis of phospho-γH2AX foci (Fig. 1G) and the comet assay (Supplementary Fig. S5C). Cisplatin is known to induce stress that promotes a stem cell state, while an upregulated TLS pathway leads to enhanced stemness properties and therapy resistance [30]. These results suggest that TAMs not only activate the TLS pathway for DNA lesion bypass, thereby contributing to therapy resistance and mutagenesis, but also directly enhance the stemness properties of ovarian cancer cells.

TAMs modulate the NER pathway following cisplatin treatment

Activation of the NER pathway is crucial for maintaining genome integrity. In line with the canonical role of XPC in initial DNA damage recognition and repair, studies by Wang et al. have found that XPC also inhibits antiapoptotic proteins. Consequently, overexpression of XPC sensitizes the otherwise resistant cells to cisplatin-induced apoptosis [31]. Moreover, the level of *XPC* appears to be downregulated in ovarian tumors from patients compared to normal tissues, as shown by box plot data extracted from the Gepia2 database (Supplementary Fig. S6A), along with the expression correlation (TNMplot.com) between *POLH* and *XPC* in clinical samples (Supplementary Fig. S6B). Additionally, the pan-cancer heatmap (TNMplot.com), illustrating *XPC* gene expression

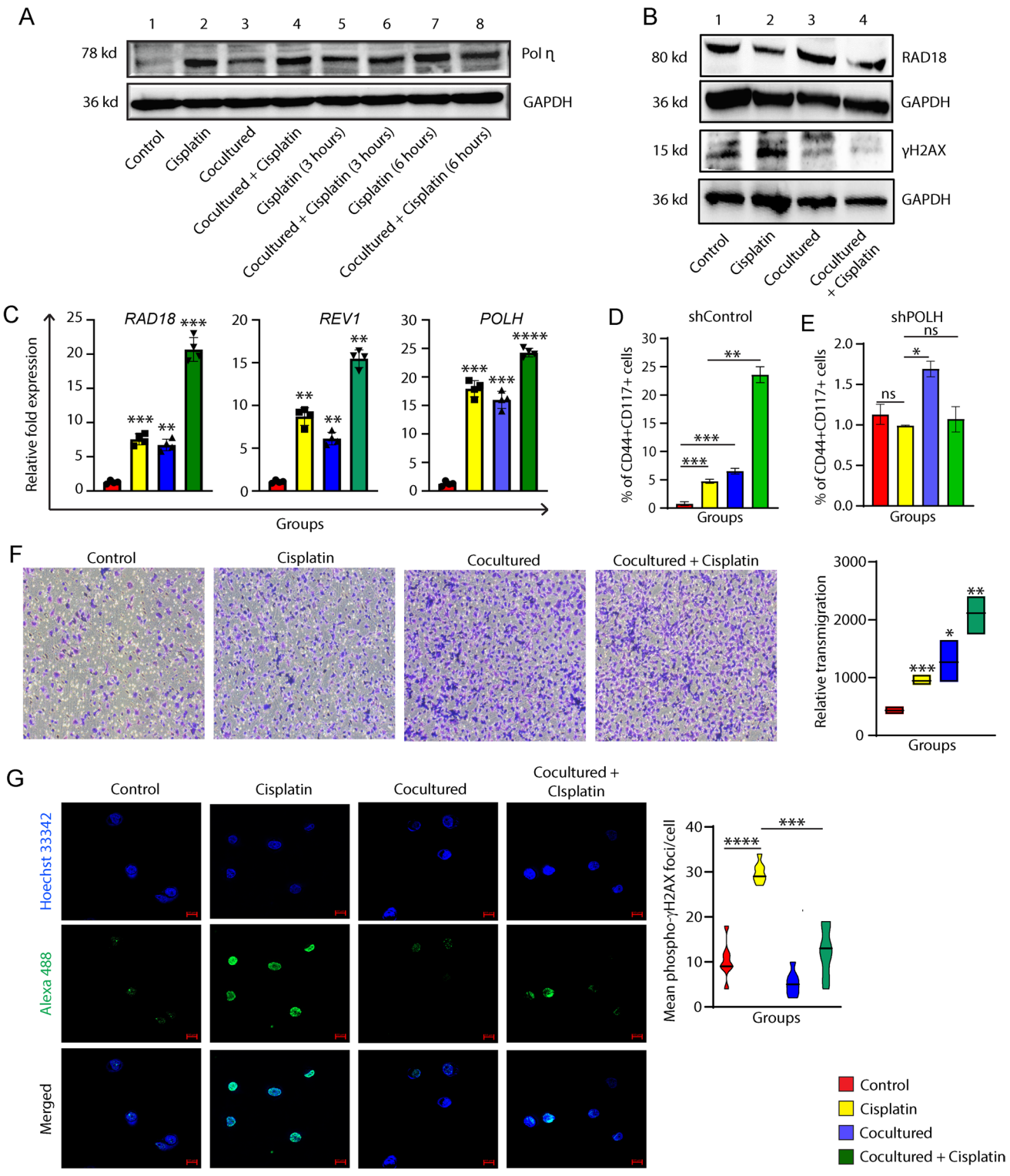

in tumor and normal tissue, revealed a similar trend (Supplementary Fig. S6C). Given XPC's dynamic role, we aimed to examine the effects of cellular crosstalk under coculture conditions between TAMs and ovarian cancer cells, both with and without cisplatin treatment. Initially, we observed that the expression level of *XPC* was lower in cocultured cancer cells compared to both control and cisplatin-treated cells (Fig. 2A, B) (Supplementary Fig. S6D). Similarly, other relevant NER-related genes, such as *XPA*, *XPB*, *XPG*, and *XPD*, were downregulated in cocultured cells at the mRNA transcript level (Fig. 2B). Interestingly, in the context of the NER

◂**Fig. 1** Cocultured cancer cells exhibit elevated Pol η expression, thereby contributing to DNA lesion bypass. (**A**) Western blot analysis of the OV2008 cell line revealed the differential expression of Pol η among the groups. Proteins from lanes 1–4 were extracted together, whereas proteins from lanes 5–6 and lanes 7–8 were extracted 3 h and 6 h, respectively, after the media was changed following cisplatin treatment. (**B**) Western blot analysis of RAD18 and phospho-γH2AX protein expression across groups. (**C**) Real-time quantitative PCR analysis of *POLH*, *RAD18*, and *REV1* expression at the mRNA level. Data represent mean ± SD of three biological replicates. (**D, E**) OVCAR3 (shControl) and OVCAR3 (shPOLH) cells were cocultured with TAMs, and the indicated groups were treated with cisplatin (20 μM) for 24 h. The percentages of CD44 + CD117 + double-positive cells were estimated. Graphs depict the average of three experimental triplicates (± SD) (**$p < 0.01$). (**F**) The transwell migration assay was performed using OVCAR3 cells. The migrated cells were stained with methylene blue (0.5 gm%) and imaged under a brightfield microscope. The experiments were performed in triplicate and are represented as mean ± SD. (**G**) Immunocytochemistry-based confocal microscopy images were developed for phospho-γH2AX foci analysis, Scale bar: 10 μm. Multiple images were taken for each group, and the number of foci/cell was calculated for each group accordingly (***$p < 0.001$, ****$p < 0.0001$). For panels C, D, E, F, and G, the Brown-Forsythe ANOVA test followed by Games-Howell's multiple comparisons test was performed

pathway, the DNA repair kinetics study indicated that the elevated level of XPC persisted in cisplatin-treated cancer cells even 6 h after media replacement. However, under coculture conditions, XPC is not only less activated by cisplatin treatment but also rapidly returns to its baseline level (Fig. 2A). Resistance to platinum-based chemotherapeutic drugs is frequently attributed to enhanced cancer stemness properties. Notably, XPC has been shown to downregulate SOX2, a stem cell-specific transcription factor, thereby reducing cancer stemness [32]. Consequently, reduced XPC induction in cocultured cells may contribute to sustained SOX2 expression and enhanced chemoresistance. In fact, the diminished expression of XPC is linked to poor patient outcomes, underscoring its potential role as both a therapeutic target and prognostic marker [33]. In terms of DNA damage recognition, class 1 HDACs (mainly HDAC1 and 2) are known to be recruited to the DNA damage sites in cells to facilitate DNA repair. HDAC inhibitors have shown promising results in overcoming chemoresistance in certain cancers [34]. Another study conducted by Kusakabe et al. revealed that although HDAC1 may assist in XPC recruitment, their knockdown does not influence XPC activity in response to DNA damage [35]. Therefore, we assessed the status of HDAC1 under our coculture conditions, and found that it was slightly elevated in cocultured cells (Supplementary Fig. S6E). Immunocytochemistry analysis of HDAC1 also indicated enhanced nuclear localization under coculture conditions (Supplementary Fig. S6F). Furthermore, activation of the NER pathway may induce apoptosis depending on the extent and pattern of the DNA lesion. In response to DNA damage, XPC potentially activates p53, thereby leading to cell cycle arrest and/or apoptosis [36]. While investigating the same function of XPC in our experimental setup, we noted reduced expression of p53 and phospho-chk2 even in cisplatin-treated and untreated cocultured cells compared to cisplatin-treated and control cancer cells (Fig. 2C) (Supplementary Fig. S6D).

Several earlier studies have indicated that activated MAPK functions as a double-edged sword in relation to cancer cell proliferation and apoptosis [37]. Some research has shown that, during increased nuclear activity and cytotoxicity, activated ERK1/2 positively regulates the NER pathway [38]. However, in our study, phospho-ERK1/2 was downregulated in the cocultured group compared to the control group (Supplementary Fig. S6D). This finding suggests that preventing the activation of apoptotic pathways in response to cisplatin may explain the downregulation of MAPK under coculture conditions. To support these data, we conducted flow cytometry analysis of phospho-γH2AX-positive cells across the four groups (Fig. 2D). The live/dead assay indicated the percentage of PI-positive cells (Fig. 2E), and cell cycle analysis (Fig. 2F) was performed for the same groups. The results demonstrated that not only was the percentage of apoptotic cancer cells following cisplatin treatment lower under cocultured conditions, but also the extent of DNA damage, as evidenced by the reduced phospho-γH2AX levels and the percentage of cells in the G0 phase in the cell cycle progression analysis.

Phenotypic characterization of THP1-derived and mouse bone marrow-derived primary macrophages cocultured with ovarian cancer cells

Similar to other gynecological malignancies, the progression of ovarian cancer is directly correlated with tumor-infiltrating macrophages that intricately communicate with cancer cells present in ascitic fluid. The characterization of subpopulations, broadly reflected by the M1/M2 ratio, determines the stage and aggressiveness of ovarian cancer. Furthermore, various patient cohort studies have identified COX2+ and CD163+ TAMs as effective predictors of poor prognosis [39]. Thus, in our study, we aimed to characterize the THP1-derived macrophages in a coculture setup. Given that the therapy-resistant phenotype of solid tumors is significantly influenced by M2 (alternatively activated) macrophages, we sought to analyze the percentage of the M2 population in our coculture setup. CD163+ and CD206+ cells were identified from THP1-derived differentiated M0 macrophages induced with PMA treatment (100 nM for 48 h), as well as from macrophages derived from the coculture

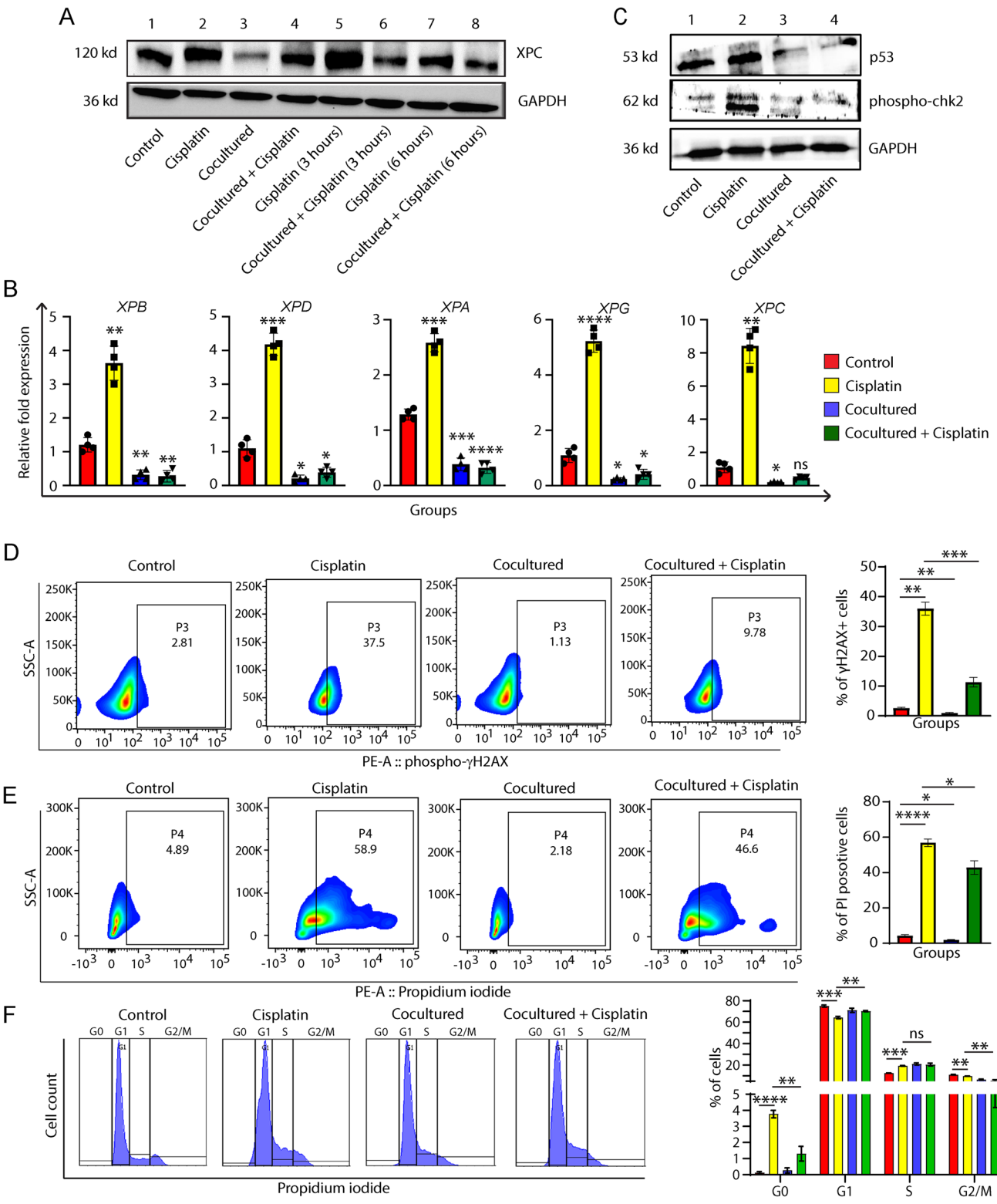

setup with and without cisplatin treatment. The number of M2-like macrophages was notably higher in the cocultured group compared to the M0 macrophage group, and even greater in the cisplatin-treated group (Fig. 3A). It is important to note that circulating undifferentiated monocytes in vivo are attracted to the tumor microenvironment through a chemokine gradient created by cancer cells, gradually differentiating into tumor-associated macrophages with varying levels of immunosuppressive phenotype [40]. Similar phenomena were observed under

◂**Fig. 2** TAMs, when cocultured with cancer cells, modulate the NER pathway in the cancer cells, following cisplatin treatment. (**A**) Western blot analysis showing the differential expression of XPC among the groups in the OV2008 cell line. Proteins from lanes 1–4 were extracted together, whereas proteins from lanes 5 and 6, and lanes 7 and 8, were extracted 3 h and 6 h, respectively, after the media was changed following cisplatin treatment. (**B**) Real-time PCR analysis of *XPC*, *XPA*, *XPB*, *XPD*, and *XPG* gene expression. mRNAs levels were normalized to *GAPDH*, and the fold changes in expression are presented as the means ± SD. The experiment was performed in triplicate (**$p < 0.01$, ***$p < 0.001$, ****$p < 0.0001$). (**C**) Western blot analysis of p53 and phospho-CHK2 protein expression in OV2008 cells across groups. (**D**) OV2008 cells were seeded and cocultured with THP1 cells for 48 h, followed by cisplatin treatment (20 μM) for 24 h. The percentage of phospho-γH2AX-positive cells was estimated. The graphical data represent the average of three replicates (***$p <$ 0.001, ****$p <$ 0.0001). (**E**) A live/dead assay was performed via flow cytometry in OV2008 cell line to estimate the number of PI-positive dead cells among the groups. The data were generated in triplicate (**$p < 0.01$, ***$p < 0.001$, and ****$p < 0.0001$). (**F**) OV2008 cells were seeded and cocultured for flow cytometry-based cell cycle analysis. The experiments were performed in triplicate (**$p < 0.01$, ***$p < 0.001$, ****$p < 0.0001$). For panels B, D, E, F, Brown-Forsythe ANOVA test followed by Games-Howell's multiple comparisons test was performed

in vitro conditions when THP1 monocytes were cultured in ovarian cancer cell conditioned media (CM) for 72 h, revealing a substantial proportion of differentiated macrophages exhibiting an M2-like phenotype. Notably, the percentage of M2 macrophages increased further with cisplatin treatment, as demonstrated by immunocytochemistry analysis (Fig. 3B) (Supplementary Fig. S7). Phenotypic differences were also evident in brightfield images, indicating a higher presence of M2-like cells in differentiated macrophages cultured in CM (Supplementary Fig. S8A). A pan-cancer heatmap illustrating the correlation among immune cell infiltration and the expression of Pol η and XPC in cancer cells revealed a predominance of immunosuppressive cell types associated with Pol η expression, whereas, an opposite trend was observed for XPC (Supplementary Fig. S8B). To further validate the results with primary cells, we successfully isolated BMDMs (Supplementary Fig. S8C) and cocultured them with the ID8 cell line for 7 days using a transwell insert system. Bright-field images of cocultured BMDMs were acquired on the 0 th, 2nd, and 5 th days (Fig. 3C). We established two groups of BMDMs: one cultured in complete DMEM media and the other cocultured with ID8 cells. The percentage of double-positive (mouse-specific CD163+ and CD206+) M2 macrophages was elevated under coculture conditions, as demonstrated by flow cytometry (Fig. 3D). In this experimental setup, an additional group was included: BMDMs cocultured with ID8 cells for 5 days, followed by cisplatin treatment (20 μM) for 24 h. Three groups were analyzed for immunocytochemistry of the CD206+ expression level in macrophages (Supplementary Fig. S8D). The results indicated a significant upregulation of CD206 expression in BMDMs cocultured with ID8 cancer cells, which further increased following cisplatin treatment. These findings provide insights into the dynamic phenotypic changes and differentiation of monocytes into TAMs, both in cell lines and primary macrophages, before and after chemotherapeutic drug treatment. These results also highlight a strong correlation between M2-like macrophages' abundance and increased expression of TLS-related genes in ovarian cancer cells, ultimately contributing to improved DNA repair capacity.

Nuclear translocation and activation of p65/RelA trigger recruitment of Pol η in cocultured ovarian cancer cells

To better understand the regulatory mechanisms of DNA repair under coculture conditions, we investigated the upstream signaling pathways involved. Additionally, we must explore the potential modulators of DNA repair pathways that are differentially regulated under coculture conditions. Research has revealed the involvement of various transcription factors, such as c-MYC, GLI, and p53, in regulating the specific DNA damage response and, therefore, the tolerance of cancer cells to the application of chemotherapeutic agents [41]. NF-κB serves as a master transcription factor and is involved in chronic inflammation, immune cell polarization, cancer cell proliferation, angiogenesis, and apoptosis [42]. It is activated in response to genotoxic stress and double-strand DNA breaks, a phenomenon that, in certain cancers, correlates with poor prognosis [43]. To track the cellular localization of p65, we performed immunocytochemistry analysis of the cancer cells. The nuclear localization of the p65 protein was greater in the cisplatin-treated group than in the control group. Surprisingly, the localization was quite high in cocultured conditions, even without cisplatin treatment, which still increased with cisplatin (Supplementary Fig. S9A). We further wanted to investigate if there was any link between the upregulated expression of Pol η and the p65 protein.

We treated the predefined groups with pristimerin (2 μM for 24 h), a well-established chemical inhibitor of IKK and IκB-α phosphorylation, thereby suppressing the phosphorylation and nuclear translocation of p65 [44, 45]. The blockade of p65 translocation with pristimerin was further validated with immunofluorescence-based staining (Supplementary Fig. S9B). The western blot data showed that, with chemical inhibition of p65, Pol η expression was lower in the cocultured lane than in the untreated lane (Fig. 4A). The clinical database GEPIA 2.0 also highlighted the positive correlation between

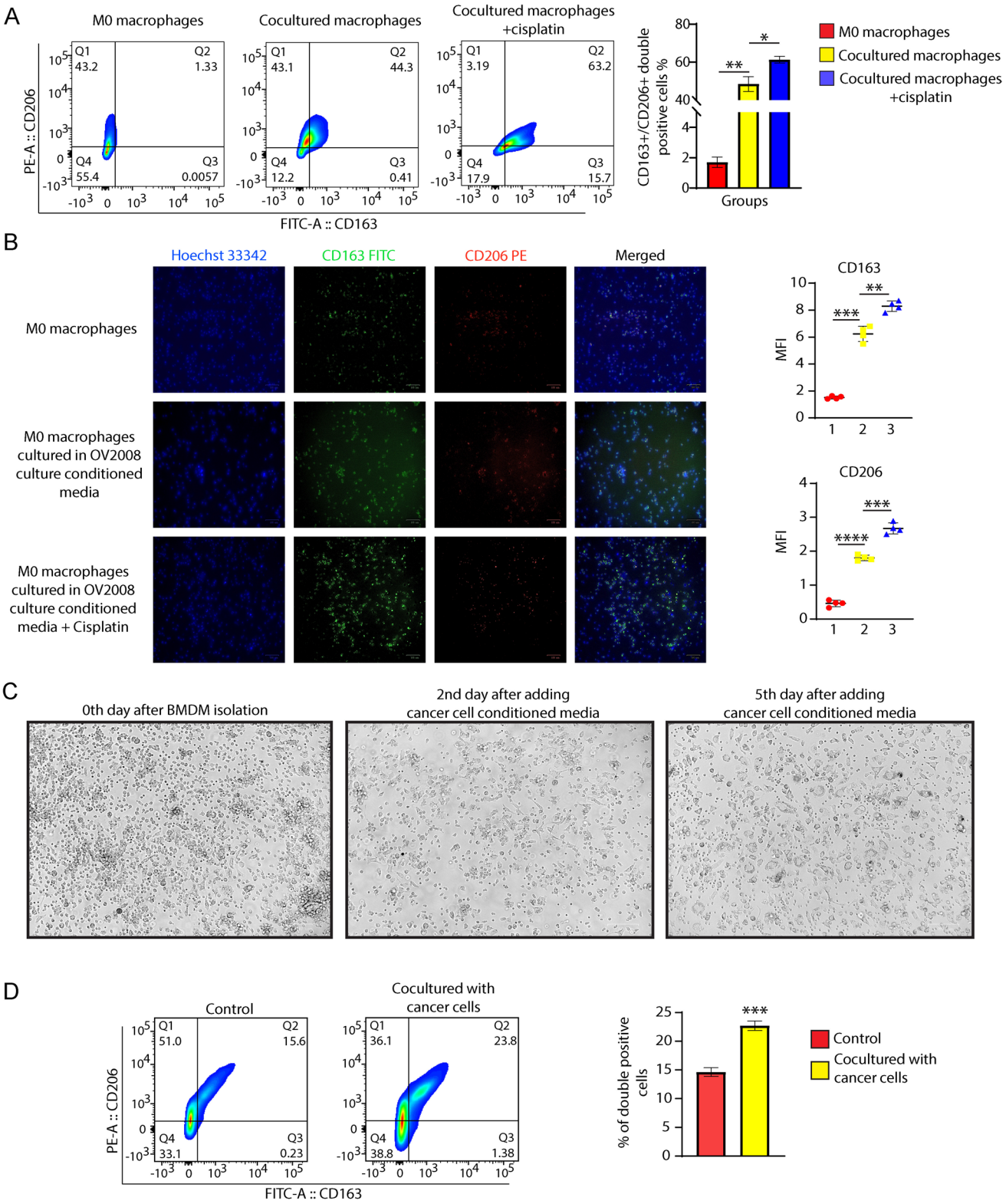
A
M0 macrophages
Cocultured macrophages
Cocultured macrophages +cisplatin
Q1 43.2
Q2 1.33
Q4 55.4
Q3 0.0057
Q1 43.1
Q2 44.3
Q4 12.2
Q3 0.41
Q1 3.19
Q2 63.2
Q4 17.9
Q3 15.7
PE-A :: CD206
FITC-A :: CD163
CD163+/CD206+ double positive cells %
Groups
M0 macrophages
Cocultured macrophages
Cocultured macrophages +cisplatin
B
Hoechst 33342
CD163 FITC
CD206 PE
Merged
M0 macrophages
M0 macrophages cultured in OV2008 culture conditioned media
M0 macrophages cultured in OV2008 culture conditioned media + Cisplatin
CD163
CD206
MFI
C
0th day after BMDM isolation
2nd day after adding cancer cell conditioned media
5th day after adding cancer cell conditioned media
D
Control
Cocultured with cancer cells
Q1 51.0
Q2 15.6
Q4 33.1
Q3 0.23
Q1 36.1
Q2 23.8
Q4 38.8
Q3 1.38
PE-A :: CD206
FITC-A :: CD163
% of double positive cells
Control
Cocultured with cancer cells

◂**Fig. 3** Phenotypic characterization of THP1-derived and mouse bone marrow-derived primary macrophages cocultured with ovarian cancer cells. (**A**) THP-1 cells were treated with PMA (100 nM) for 24 h to induce differentiation, followed by coculture with ovarian cancer cells (OV2008) for 48 h. Cisplatin treatment (20 μM) was applied to the respective groups for 24 h, following the first 24 h of coculture. The cells were analyzed by flow cytometry for the percentage of CD163+ CD206+ THP-1-derived M2-like macrophages. Each experiment was performed in triplicate (**$p < 0.01$, *$p < 0.05$). (**B**) Immunocytochemical staining of live cells seeded on coverslips was performed using FITC-tagged CD163 and PE-tagged CD206 antibodies to identify M2-like macrophages. The nuclei were counterstained with Hoechst 33342 dye, and images were acquired using a fluorescence microscope (scale bar = 100 μm). The graph shows fluorescence intensity (mean ± SD) from three independent experiments. *$p < 0.05$, **$p < 0.01$. Group key: 1- M0 macrophages, 2- Macrophages cocultured with conditioned media (CM), 3-Macrophages cocultured with CM + Cisplatin, Scale bar: 100 μm. (**C**) Mouse bone marrow-derived primary macrophages (BMDMs) were cultured for 7 days for optimal differentiation with mouse ID8 cell line-conditioned media. Images were acquired at different time points, as indicated in the figure, under a brightfield microscope, Scale bar: 80 μm. (**D**) Flow cytometric assessment of M2 polarization in mouse BMDMs based on CD163+ CD206+ double-positive populations after 5 days in control media or mouse ovarian cancer cell-conditioned media. Bar graph shows quantification from three replicates (***$p < 0.001$). For panels A and B, the Brown-Forsythe ANOVA test followed by Games-Howell's multiple comparisons test was performed. For panel D, an unpaired Student's t-test was performed

RELA (p65) expression and *POLH* (Pol η) in tumor tissues (Fig. 4B). Immune cell infiltration at the pan-cancer level was associated with increased *RELA* (p65) expression in cancer cells, and a heatmap indicated a positive correlation between M2 macrophages and the Treg cell population and p65 expression (Fig. 4C) [46]

Finally, we investigated whether activated p65 can bind to the promoter region of *POLH* and regulate the gene at the transcriptional level. ChIP−qPCR was conducted using two different primers designed for the promoter sequence of Pol η, derived from the EPD database (Supplementary Fig. S10A) (https://epd.ExPASy.org/epd/). We found that, compared to the control group, the binding of p65 to the promoter region of the Pol η gene in the cisplatin-treated group was enhanced. Moreover, under coculture conditions, we still detected increased p65 binding even without cisplatin treatment (Fig. 4D, E). Summarizing our findings regarding p65 expression dynamics, we assert that the elevated expression of p65 under cocultured conditions may regulate Pol η expression at the transcriptional level. To identify potential mediators of p65 activation in cancer cells under coculture conditions, we performed a membrane-based cytokine array using conditioned media from the four groups. The expression of key cytokines and chemokines, such as IL8, CXCL10, CXCL1, and SERPIN E1, increased under coculture conditions (Fig. 4F). Since these cytokines can activate the NF-κB pathway, we can predict a possible p65 activation process in cocultured cancer cells. However, further research is needed to establish the potential mediator link with p65 activation.

Modulation of the DNA damage response in an ovarian cancer xenograft model

Having validated our findings in vitro, we next aimed to asses the correlation between M2-like TAMs and DNA damage repair activation in response to cisplatin treatment in vivo. Hence, we developed a human xenograft tumor model in immunocompromised mice as illustrated in Fig. 5A. Tumor weight analysis revealed that in the shControl background, co-injection of OVCAR3 cells with THP1 cells significantly increased tumor growth compared to the control group (OVCAR3 shControl alone). Cisplatin treatment alone led to a significant reduction in tumor weight; however, this antitumor effect was partially resisted by THP1 co-injection, as tumor weight in the THP1 + cisplatin group remained significantly higher than in the cisplatin-only group. This indicates that THP1-derived macrophages conferred partial resistance to cisplatin in the shControl setting. In the shPOLH background, cisplatin treatment remarkably reduced tumor weight compared to both the shControl cisplatin and shControl co-injected groups. Notably, there was no statistically significant difference in tumor weight between the cisplatin-only and THP1 + cisplatin-treated groups, suggesting that *POLH* knockdown may attenuate the macrophage-mediated chemoresistance observed in the shControl context. (Fig. 5B). Moreover, histological changes in the tumor tissues indicated partially disrupted tissue integrity in the cisplatin-treated group, but this alteration was not evident in the treatment of the co-injected group (Supplementary Fig. S10B). Blood collected from the retro-orbital plexus of the mice was utilized to estimate the levels of key cytokines across all relevant groups. We observed a significant increase in the IL-6 level in the OVCAR3 (shControl) + THP1 co-injected group compared to the control group, which was further amplified with cisplatin treatment. However, the increase was minimal in the OVCAR3-shPOLH + THP1 co-injected group, even with cisplatin treatment (Supplementary Fig. S10C). While IL-6 is linked to cancer stemness, angiogenesis, and DNA damage repair, its primary role is to activate the NF-κB transcription factor [47, 48]. We found that this elevated IL-6 level was highly pertinent to our study.

Immunofluorescence staining using Arginase 1 and CD206 primary antibodies highlighted differentiated macrophages in the OVCAR3-(shcontrol) + THP1 co-injected group, exhibiting the M2-like phenotype. The images confirmed that the M2-like macrophage population was larger in the cisplatin-treated co-injected group compared to the untreated group. These findings validated the in vitro

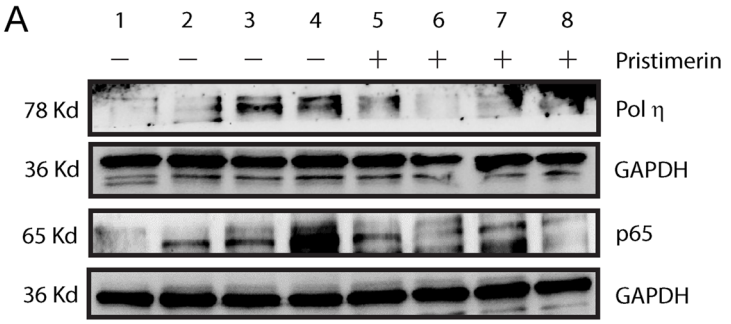
A
1 2 3 4 5 6 7 8
— — — — + + + +
Pristimerin
78 Kd
Pol η
36 Kd
GAPDH
65 Kd
p65
36 Kd
GAPDH

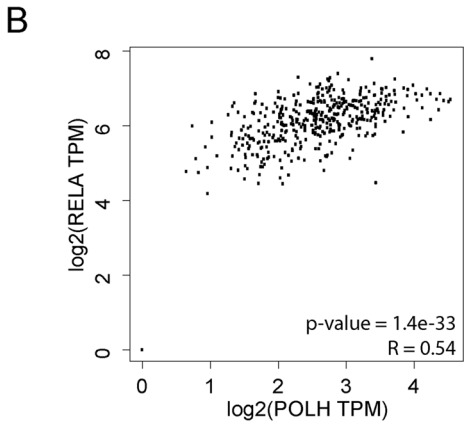
B
log2(RELA TPM)
log2(POLH TPM)
p-value = 1.4e-33
R = 0.54

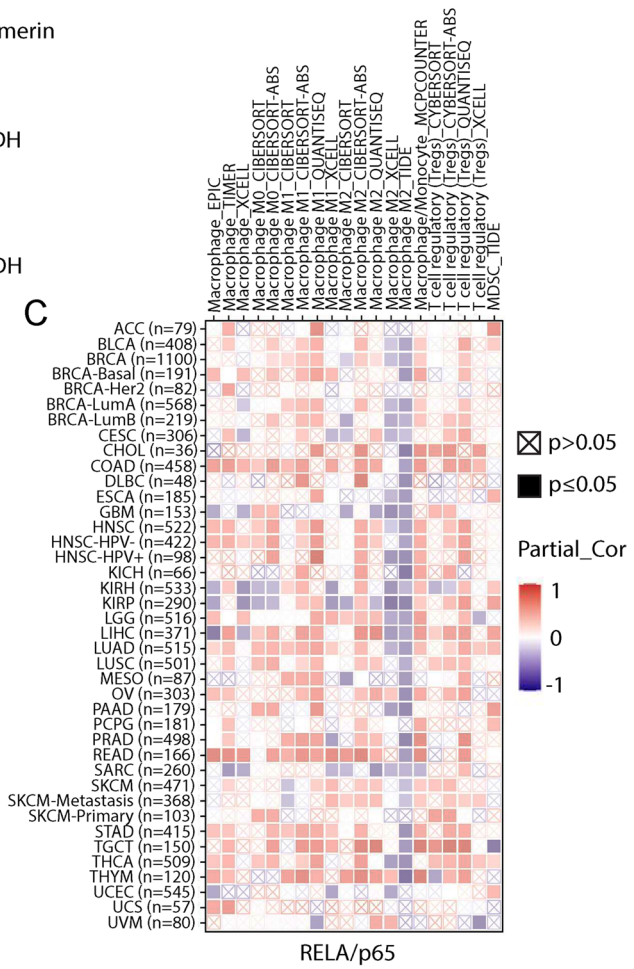
C
Macrophage_EPIC
Macrophage_TIMER
Macrophage_XCELL
Macrophage M0_CIBERSORT
Macrophage M0_CIBERSORT-ABS
Macrophage M1_CIBERSORT
Macrophage M1_CIBERSORT-ABS
Macrophage M1_QUANTISEQ
Macrophage M1_XCELL
Macrophage M2_CIBERSORT
Macrophage M2_CIBERSORT-ABS
Macrophage M2_QUANTISEQ
Macrophage M2_XCELL
Macrophage M2_TIDE
Macrophage/Monocyte_MCPCOUNTER
T cell regulatory (Tregs)_CYBERSORT
T cell regulatory (Tregs)_CYBERSORT-ABS
T cell regulatory (Tregs)_QUANTISEQ
T cell regulatory (Tregs)_XCELL
MDSC_TIDE
ACC (n=79)
BLCA (n=408)
BRCA (n=1100)
BRCA-Basal (n=191)
BRCA-Her2 (n=82)
BRCA-LumA (n=568)
BRCA-LumB (n=219)
CESC (n=306)
CHOL (n=36)
COAD (n=458)
DLBC (n=48)
ESCA (n=185)
GBM (n=153)
HNSC (n=522)
HNSC-HPV- (n=422)
HNSC-HPV+ (n=98)
KICH (n=66)
KIRH (n=533)
KIRP (n=290)
LGG (n=516)
LIHC (n=371)
LUAD (n=515)
LUSC (n=501)
MESO (n=87)
OV (n=303)
PAAD (n=179)
PCPG (n=181)
PRAD (n=498)
READ (n=166)
SARC (n=260)
SKCM (n=471)
SKCM-Metastasis (n=368)
SKCM-Primary (n=103)
STAD (n=415)
TGCT (n=150)
THCA (n=509)
THYM (n=120)
UCEC (n=545)
UCS (n=57)
UVM (n=80)
p>0.05
p≤0.05
Partial_Cor
1
0
-1
RELA/p65

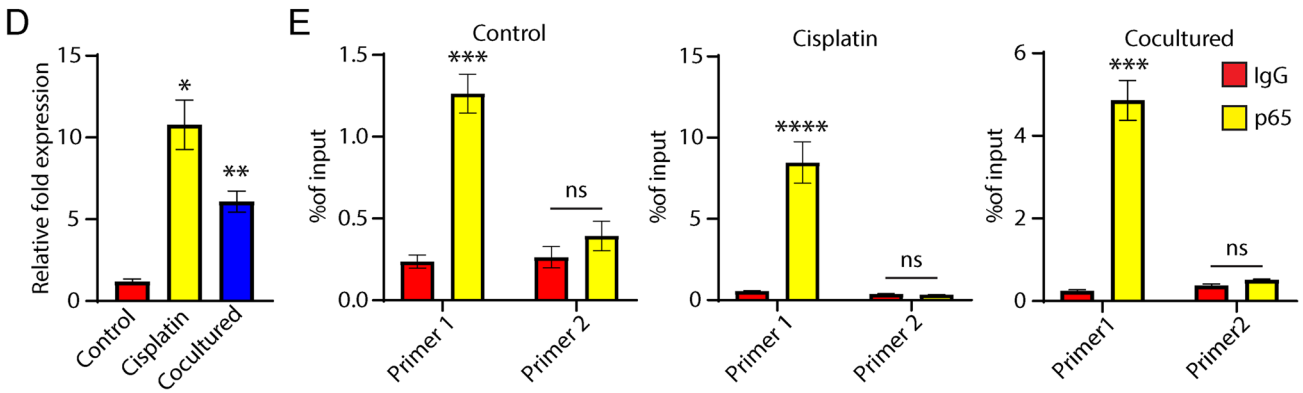
D
Relative fold expression
Control
Cisplatin
Cocultured
E
Control
Cisplatin
Cocultured
%of input
Primer 1
Primer 2
IgG
p65
ns

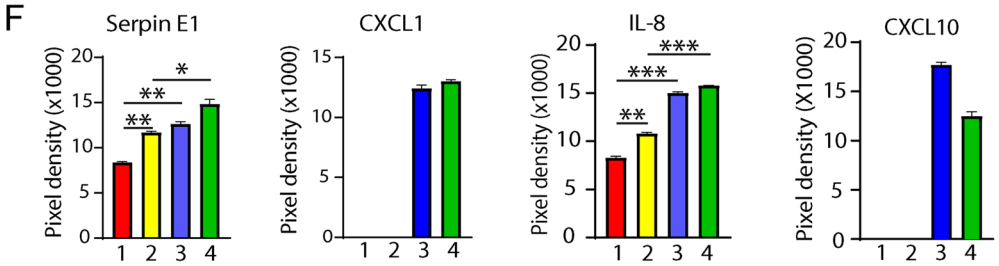
F
Serpin E1
CXCL1
IL-8
CXCL10
Pixel density (x1000)
Pixel density (X1000)

◂**Fig. 4** Tumor-associated macrophages enhances p65 activity in ovarian cancer cells. (**A**) Western blot analysis showing the effect of pristimerin (2 μM for 24 h), a selective p65 blocker, on Pol η and p65/RelA expression in OVCAR3 cells. Lanes 1–4 represent control, cisplatin treated, cocultured, and cocultured + cisplatin-treated cells, respectively, whereas lanes 5–8 mimics lanes 1–4 with an additional pristimerin treatment prior to cisplatin (20 μM, 24 h) treatment. GAPDH was used as loading control. Group keys: 1&5-Control, 2&6- Cisplatin, 3&7- Cocultured cells, 4&8- Cocultured cells + Cisplatin. (**B**) The scatter plot illustrates the Spearman correlation between *POLH* and *RELA* (p65) gene expression in ovarian cancer patient samples (n > 400; TCGA OV tumor), based on RNA-Seq data. The analysis reveals a strong positive correlation (R = 0.54) with a highly significant p-value (1.4×10^{-33}), indicating that increased *RELA* expression is associated with elevated *POLH* expression in ovarian tumors. (**C**) Heatmap extracted from the TIMER 2.0 database depicting the pan-cancer correlation between *RELA* expression and immune cell subpopulation infiltration in tumors. (**D**, **E**) OV2008 cells were harvested for ChIP−qPCR with anti-p65 antibody. Two primers were designed using the *POLH* promoter region for the p65 antibody binding-based ChIP assay. Graph depicting the relative fold change in p65 binding in the promoter region of *POLH*. ChIP data graphically represent the percent input level. The experiments were performed in triplicate, and the results are presented as means ± SD. (**F**) A membrane-based cytokine array was performed with cultured media from different groups. Graphical representation of the differential expression levels of key cytokines. $*p < 0.05$, $**p < 0.01$, $***p < 0.001$, $****p < 0.0001$. Group keys: 1- Control, 2- Cisplatin, 3- Cocultured cells, 4- Cocultured cells + Cisplatin

observations of increased M2 marker expression following cisplatin treatment (Fig. 5C). To estimate the extent of DNA damage, IHC and immunofluorescence analysis of phospho-γH2AX yielded distinct results (Fig. 5D). The expression was lower in the cisplatin-treated THP1 + OVCAR3 (shControl) co-injected group than in the cisplatin-treated OVCAR3 (shControl) group (Supplementary Fig. S11). Additionally, the expression of proliferative markers, such as Ki67, appeared to be slightly higher in the co-injected group compared to the control group (Fig. 5E).

For solid tumors, the longstanding paradigm is that lymph node metastasis serves as a starting point for future systemic tumor spread [49]. Furthermore, immune cell infiltration from the tumor microenvironment into lymph nodes results in tumor-educated drainage nodes, which ultimately dictate the systemic response to malignant progression [50, 51]. Therefore, in this study, we isolated inguinal drainage lymph nodes for immunofluorescence imaging of the cisplatin-treated and untreated co-injected groups (OVCAR3-shcontrol + THP1) to identify migrated macrophages with an M2-like phenotype. In the co-injected group, human-specific Arginase 1 + and CD206 + positive cells were localized specifically near the subcapsular sinus area of the lymph node (Supplementary Fig. S12A, B). The infiltration of M2-phenotype macrophages further increased with cisplatin treatment, reflecting the heightened presence of tumor-educated lymph nodes and the immune tolerance facilitated by M2 macrophages in response to cisplatin treatment, thereby contributing to chemoresistance. Additionally, confocal images showed an elevated level of p65 in the co-injected group compared to the control group. Subsequently, cisplatin treatment further increased the nuclear expression (Supplementary Fig. S13).

Correlation of Pol η expression with the M2 macrophage population in clinical samples

To get some clinical perspective, we obtained clinical samples of ovarian tumors (treatment-naïve) from the Chittaranjan National Cancer Institute, India. As described in the schematic diagram (Fig. 6A), we processed one part of the patient-derived tumor tissues and adjacent noncancerous ovarian tissues for flow cytometry analysis of the M2-like macrophage population assessment and the other part for parafilm-embedded tissue sectioning for immunofluorescence. Flow cytometry analysis of human-specific CD163+ and CD206+ M2 phenotypic markers revealed a greater presence of M2-like macrophages in tumor tissues than in adjacent noncancerous tissues (Fig. 6B). To determine Pol η expression in clinical samples, we performed immunofluorescence staining of the tissue sections. The images support our previous findings that patient-derived tumor tissues express a greater level of Pol η than noncancerous ovarian tissue (Fig. 6C, D), which is positively correlated with elevated M2-like macrophage infiltration.

Macrophage population correlation with the chemoresistance phenotype of ovarian cancer patients

A publicly available ovarian cancer dataset was used for scRNA-seq analysis to investigate immune and malignant cell populations associated with chemoresistance.. In the GSE184880 dataset, a total of 33,846 cells (nonmalignant: 15,937 cells and malignant: 17,909 cells) were preprocessed, and following quality control and normalization, dimensionality reduction was performed using the top 20 principal components. Subsequently, single-cell transcriptomes were clustered into 22 distinct groups using the FindNeighbors and FindClusters functions in Seurat, with a dimensional range of 1 to 20 and a resolution parameter of 0.5. Cell types were annotated by using the expression of known marker genes (Fig. 7A, B). Among the total DEGs, 19 genes from the macrophage clusters and 21 genes from the cancer cell clusters were shortlisted. Genes that are

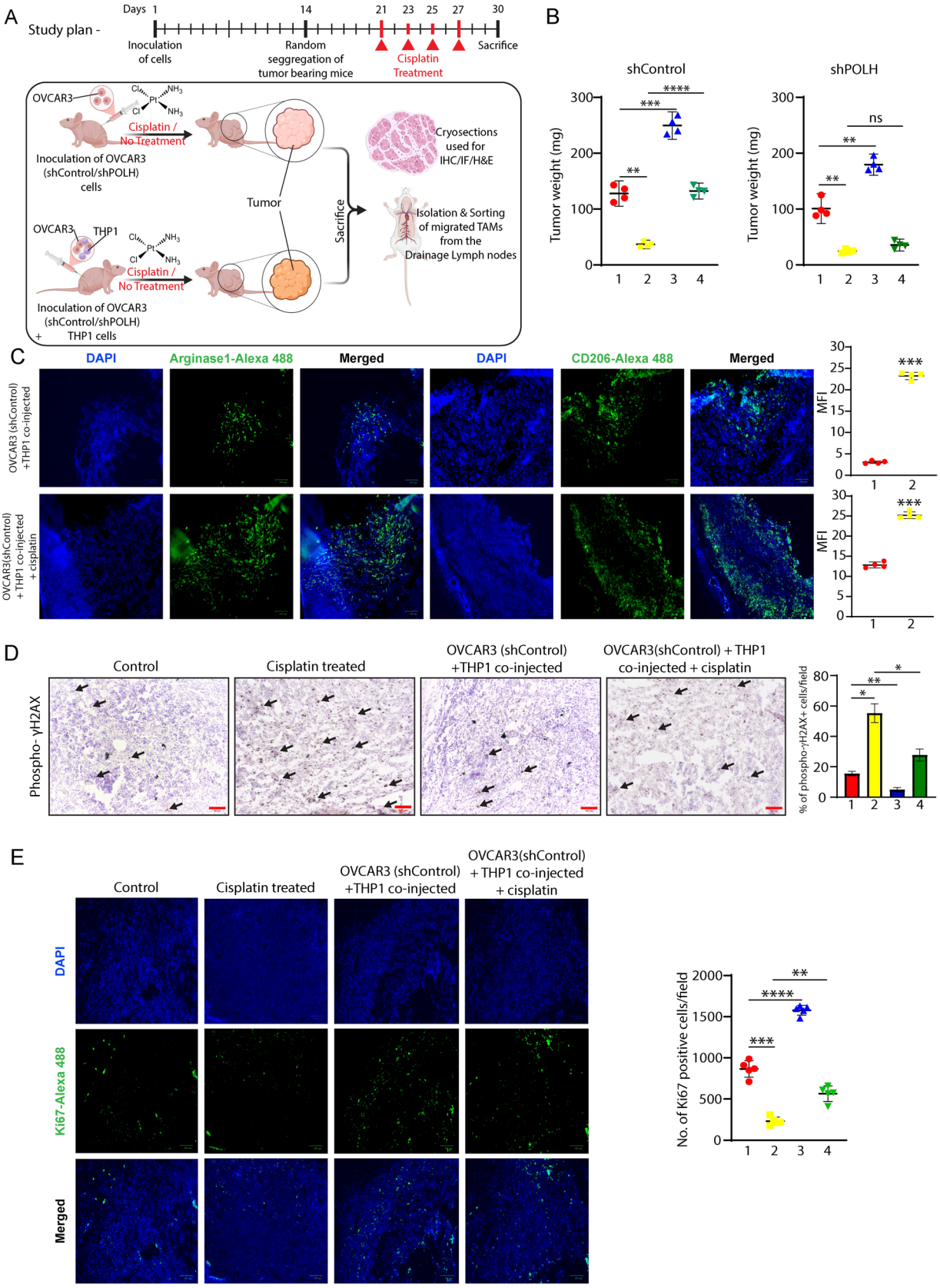
A
Study plan -
Days 1 14 21 23 25 27 30
Inoculation of cells
Random segregation of tumor bearing mice
Cisplatin Treatment
Sacrifice
OVCAR3
Cisplatin / No Treatment
Inoculation of OVCAR3 (shControl/shPOLH) cells
Tumor
Sacrifice
Cryosections used for IHC/IF/H&E
Isolation & Sorting of migrated TAMs from the Drainage Lymph nodes
OVCAR3
THP1
Cisplatin / No Treatment
Inoculation of OVCAR3 (shControl/shPOLH) + THP1 cells
B
shControl
shPOLH
Tumor weight (mg)
ns
C
DAPI
Arginase1-Alexa 488
Merged
DAPI
CD206-Alexa 488
Merged
OVCAR3 (shControl) +THP1 co-injected
OVCAR3(shControl) + THP1 co-injected + cisplatin
MFI
D
Control
Cisplatin treated
OVCAR3 (shControl) +THP1 co-injected
OVCAR3(shControl) + THP1 co-injected + cisplatin
Phospho- γH2AX
% of phospho-γH2AX+ cells/field
E
Control
Cisplatin treated
OVCAR3 (shControl) +THP1 co-injected
OVCAR3(shControl) + THP1 co-injected + cisplatin
DAPI
Ki67-Alexa 488
Merged
No. of Ki67 positive cells/field

◂**Fig. 5** In vivo studies using OVCAR3 shControl and OVCAR3 shPOLH stable cell lines – (**A**) Schematic representation of the in vivo experimental design. Athymic nude mice were subcutaneously injected with OVCAR3 (shControl) or OVCAR3 cells with Pol η knockdown (shPOLH). In the indicated groups, THP1-derived monocytes were co-injected. Mice were treated with cisplatin or left untreated, and tumors were harvested after ≈4 weeks (30 days) for downstream analyses. (**B**) Tumor weights from the different groups of athymic nude mice were measured at the endpoint. Data are presented as the means ± SD for each group: 1 – Control (OVCAR3 shControl/shPOLH, untreated), 2 – Cisplatin-treated (OVCAR3 shControl/shPOLH), 3 – OVCAR3 (shControl/shPOLH) + THP1 co-injected, untreated, 4 – OVCAR3 (shControl/shPOLH) + THP1 co-injected + cisplatin-treated. Tumor weights are presented as mean ± SD. Statistical analysis was performed using Brown-Forsythe ANOVA followed by Games-Howell's multiple comparisons test (**p < 0.01, ***p < 0.001, ****p < 0.0001, ns = not significant). (**C**) Immunofluorescence images of the cryosections of the tumor samples from the OVCAR3(shcontrol) + THP1 coinjected group (1) and OVCAR3(shcontrol) + THP1 coinjected + cisplatin group (2) were generated via anti-Arginsase-1 and anti-CD206 primary antibodies for M2-like macrophage detection. Subsequently, an Alexa Fluor-488-conjugated anti-rabbit secondary antibody was used for the detection of the primary antibody. The staining procedures were performed in triplicate. Mean fluorescence intensity (MFI) was quantified and shown as mean ± SD. Scale bar = 100 µm. Statistical analysis: unpaired Student's t-test (*p< 0.001). (**D**) Tumor sections were subjected to immunohistochemical staining with phospho-γH2AX antibody. Black arrows indicate γH2AX-positive cells. Accordingly, the mean gray value intensity was quantified via ImageJ software, and the graphs represent the mean± SD, scale bar = 500 µm. (**E**) Tumor cryosections were immuno-stained with a Ki67 antibody and detected with an Alexa Fluor 488-conjugated anti-rabbit secondary antibody. Pictures were taken under a fluorescence microscope. The number of ki67-positive cells was estimated via ImageJ software, and the graphical representation shows the mean ± SD number of positive cells per field for each group (5 fields/group), scale bar = 100 µm. **p< 0.01, ***p< 0.001, ****p< 0.0001. For panels B, D, E, and F, the Brown-Forsythe ANOVA test followed by Games-Howell's multiple comparisons test was performed. And for the panel C, an unpaired student's t-test was performed. Group key for panel D and E, 1- Control, 2- Cisplatin, 3-OVCAR3(shcontrol) + THP1 coinjected, 4- OVCAR3(shcontrol) + THP1 coinjected + Cisplatin

involved in the M2-like phenotype were selected from the macrophage clusters. The genes associated with poor prognosis, therapy resistance, metastasis, and invasion were selected from cancer cell clusters. The transcription levels of these shortlisted genes among the identified macrophage clusters (Fig. 7C) and the cancer cell cluster (Supplementary Fig. S14) were depicted. Additionally, differential gene expression between tumors and normal tissues at the single-cell level in macrophage clusters was also demonstrated through a UMAP plot (Supplementary Fig. S15) (Supplementary Fig. S16) (Supplementary Fig. S17A). The expression level in terms of the percentage of cells expressing the representative genes among different cell clusters is displayed as a feature plot and heatmap (Supplementary Fig. S17B, C) (Supplementary Fig. S18) (Supplementary Fig. S19). In the context of the upregulated genes in the macrophage clusters, we performed protein–protein interaction (PPI) and pathway enrichment analyses through in-silico web servers, Metascape and GeneMANIA.

The co-expression, colocalization, and physical interactions of selected genes were illustrated through PPIs, which together are involved in multiple aspects, such as negative regulation of T-cell activation and migration, myeloid cell activation, differentiation, and chemotaxis (Supplementary Fig. S20A). Pathway enrichment analysis highlighted the pathways related to innate immune cell maturation and activation (Supplementary Fig. S20B). Similarly, a PPI depiction of representative genes from cancer cell clusters is provided in Supplementary Fig. S21A. Additionally, enrichment analysis of cancer cells revealed predominant involvement in endometrioid and ovarian malignancies (Supplementary Fig. S21B). Moreover, we performed enrichment analysis of transcription factors that highlighted ELF1, AP1, PSMB5, GTF2 A2, and TAF9B (Supplementary Fig. S21C). Interestingly, almost all the transcription factors are directly or indirectly involved in the DNA damage repair pathways of cancer cells.

In summary, our single-cell transcriptomic analysis suggests a strong correlation among M2-like macrophage prevalence and enhanced DNA repair capacity, metastasis, and therapy resistance in ovarian cancer. This analysis highlighted the multilayered crosstalk between tumor-associated macrophages and cancer cells, which is consistent with our experimental findings.

Discussion

The gradual acquisition of a resistant phenotype to various chemotherapeutic agents is a result of altered cellular apoptotic pathways, enrichment of stemness properties, and increased levels of DNA damage sensors and repair proteins [52]. The functional concept of CSCs states that cells have the natural ability to resist chemo-radiotherapy due to the elevated level of multidrug resistance transporters and increased DNA repair ability [53, 54]. Cisplatin, for instance, usually enriches cancer stem-like cells upon chronic exposure through the activation of detoxifying enzymes such as ALDH and other stemness-associated genes such as *OCT4*, *SOX2*, *BMI1*, *CTNNB1* (β-catenin), and *NOTCH1* [55, 56]. Nevertheless, the primary focus is to overcome chemoresistance mechanisms through adjuvant therapy and to understand more about the dynamic crosstalk of the component cells of the TME [57].

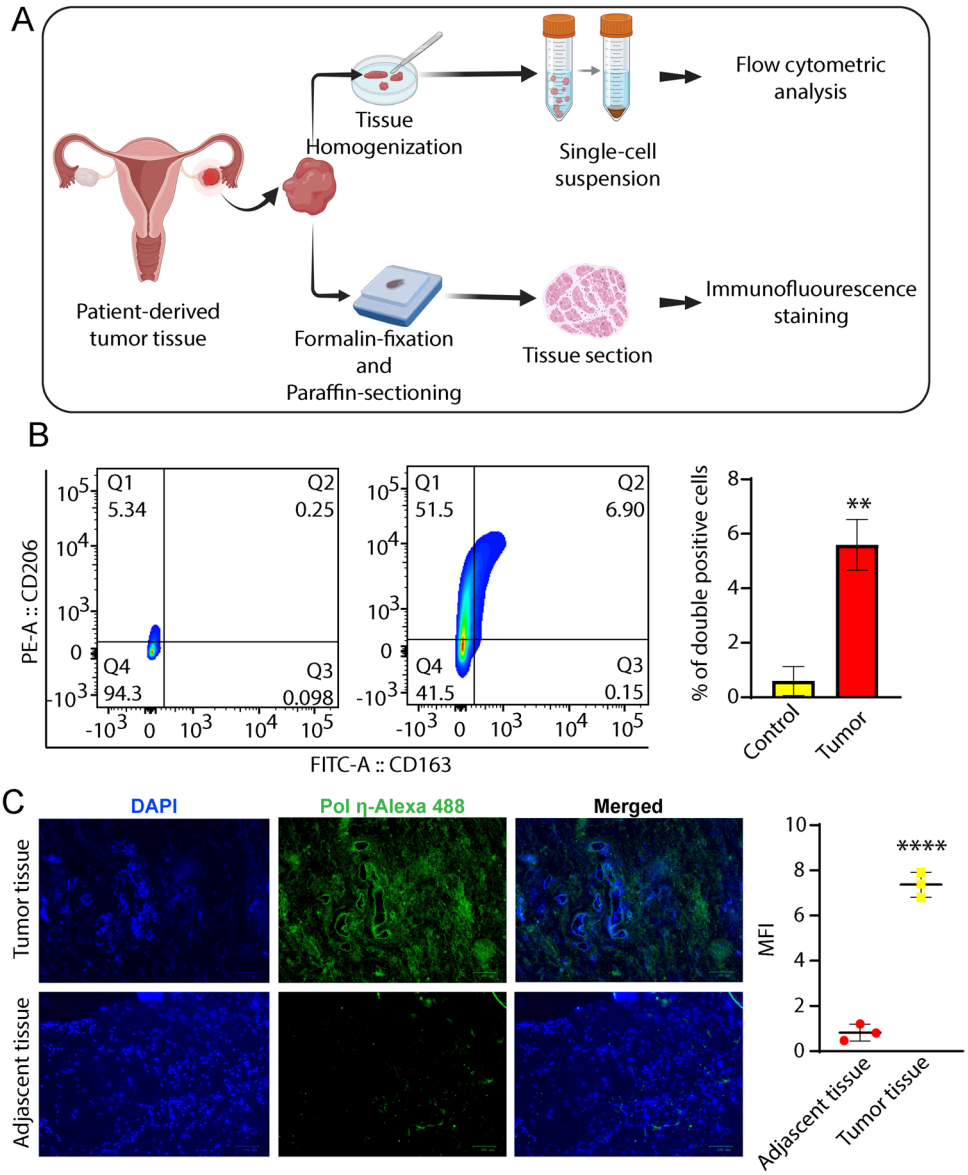

Fig. 6 Correlating the in vitro and in vivo data of the associations between Polη expression and the M2 macrophage population in clinical samples. (**A**) Schematic representation of the protocol for purifying and processing patient-derived ovarian tumor tissue for further downstream analyses. (**B**) The isolated single-cell suspensions were processed for flow cytometry analysis of CD206 + and CD163 + double-positive M2-like macrophages between cancer tissue and adjacent noncancerous ovarian tissue. The experiment was performed in triplicates, and the data are represented as mean ± SD. $^{**}p < 0.01$. (**C**) Paraffin sections of the tumor and adjacent noncancerous tissues were subjected to immunofluorescence-based staining with a Pol η-specific primary antibody. An Alexa Fluor 488-conjugated anti-rabbit secondary antibody was used to detect the Pol η level. Images of multiple tissue sections were acquired by fluorescence microscopy. The mean fluorescence intensity is depicted as the mean ± SD. $^{****}p < 0.0001$

In this study, we have furnished evidence of how cellular crosstalk between TAMs and cancer cells can directly modulate the DNA repair pathways of the latter in response to cisplatin treatment. Notably, our data indicates that cancer cells grown together with macrophages show increased expression of the *POLH* gene—which is involved in a DNA repair process called translesion synthesis —even in the absence of cisplatin. Such elevated expression of Y family polymerases enhances the mutation rate in cancer cells, driving the emergence of drug-resistant clones and enabling them to survive therapy-induced stress [58]. Further investigation revealed that the stemness properties of cancer cells are markedly enhanced in the presence of macrophages. TAMs appear to indirectly promote this enrichment by upregulating the TLS-related genes in cancer cells, an effect that becomes even more pronounced following cisplatin treatment. The role of Pol η is particularly evident, as downregulation of this gene diminished the difference in the stemness properties between the control and the cocultured cancer cells. Moreover, expression of DNA damage markers, such as phospho-γH2AX, was significantly reduced in cisplatin-treated cocultured cancer cells compared to controls. Notably, cisplatin activates the nucleotide excision repair pathway, which functions to eliminate bulky DNA adducts [59]. Within NER pathway, the initial recognition of DNA damage is executed through XPC [60]. Compared to the control, we found that XPC expression was downregulated in cocultured cells, even after cisplatin treatment. As previous studies suggest that a reduced XPC expression is directly associated with the chemoresistant phenotype in certain cancers, we further confirmed the downregulation of other

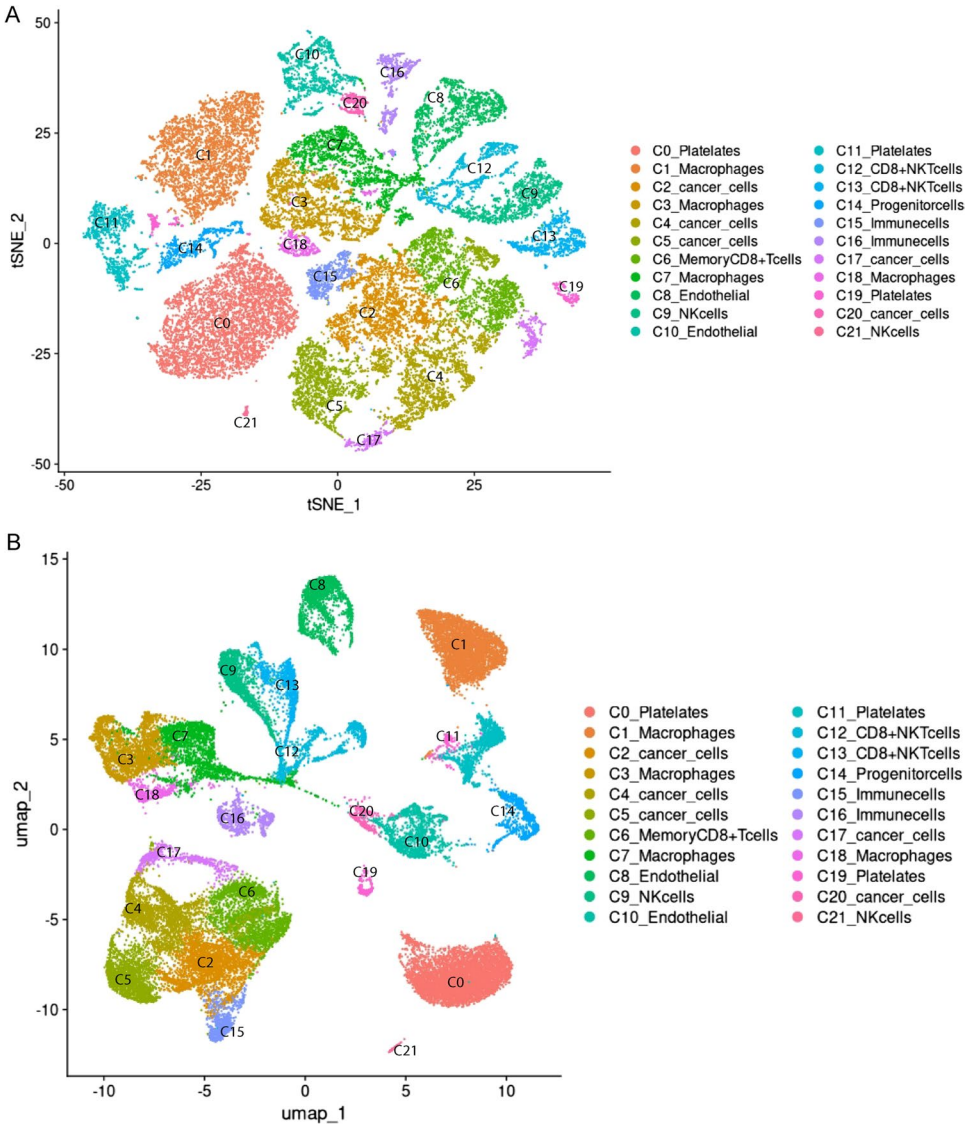

Fig. 7 Single-cell RNA sequencing data correlating ovarian cancer therapy resistance with the M2-like macrophage population. **(A, B)** UMAP and tSNE visualization of scRNA-seq clusters of ovarian cancer patients derived from the Gene Expression Omnibus dataset. (**C**) The single-cell transcription levels of representative genes associated with macrophage clusters are illustrated in UMAP plots

key genes related to the NER pathway, such as *XPA*, *XPG*, *XPD*, and *XPB,* in our study. This suppression of the NER pathway likely disrupted the activation of apoptotic signaling and cell cycle arrest mechanisms in response to cisplatin. In line with this event, we found a reduced p53 expression along with a decreased percentage of cells in the G0 and G2/M phases of the cell cycle. Since macrophages play a central role in driving these cellular responses in cancer cells, it was essential to experimentally validate their phenotype. Given the phenotypic diversity of TAMs, we characterized the majority of the macrophage population in our study as CD206+ CD163+ double-positive, alternatively activated macrophages.

Through a series of mechanistic investigations, we further identified the clear and distinctive role of RelA/p65 in the preferential induction of the TLS pathway under cocultured conditions. Because RelA/p65 is known to be activated in DNA damage repair mechanisms, we investigated its nuclear translocation under cocultured conditions. Further, ChIP−qPCR confirmed the preferential binding of p65 to the promoter region of *POLH*, thus contributing to gene regulation.

Moreover, we validated these experimental findings regarding the dynamic DNA damage response of ovarian cancer cells driven by crosstalk with TAMs using an in vivo xenograft tumor model. Since IL-6 is a known activator of the NF-κB pathway, we measured its levels in mice blood and confirmed a significant increase in the cancer cell- and monocyte-co-injected groups compared to control. However, this increase was not particularly evident in mice with tumors derived from Pol η-deficient cell line. As stated by Nejad et al., IL-6 expression is strongly correlated with a poor prognosis, chemoresistance, and immune evasion [61]. Based on our results, we

Fig. 7 (continued)

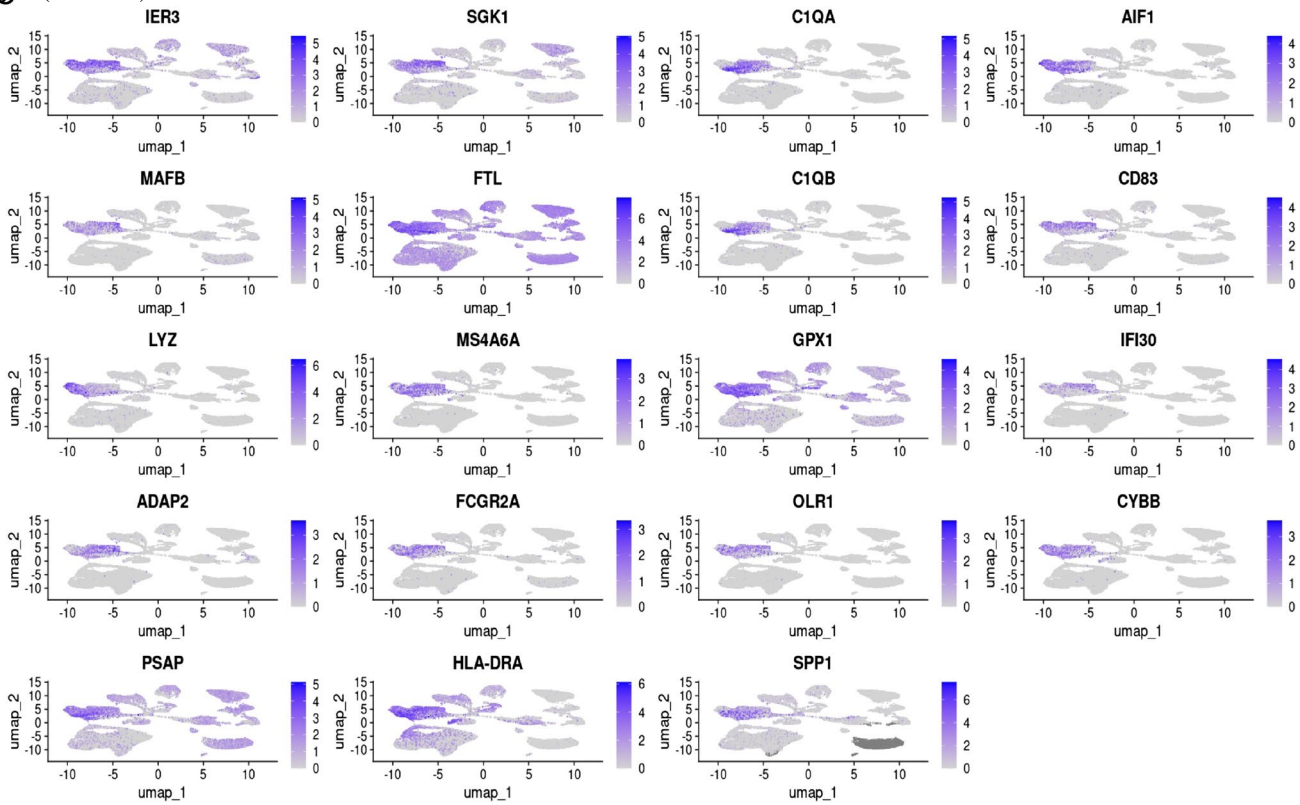

believe that IL-6 might be an important contributor to p65 activation in cancer cells, particularly when the number of immune-suppressive TAMs (M2-like) is significantly higher in the tumor microenvironment. Single-cell transcriptomics data interpretations identified chemoresistance- and metastasis-related differentially expressed genes from cancer cell clusters, and M2-like phenotype-related genes from macrophage clusters. Interestingly, transcription factor enrichment analysis of the genes from cancer cell clusters revealed that the *ELF1*, *AP1*, *PSMB5*, *GTF2A2*, and *TAF9B* genes are intricately involved in the DNA damage response of cancer cells. Therefore, the observed positive correlation between macrophage infiltration and enhanced DNA repair capacity in the clinical context of ovarian cancer appears to be well supported.

In conclusion, our findings explicitly highlight the influence of immune cells on the DNA damage response of cancer cells in the TME. The direct and complicated role of TAMs in inducing the chemoresistance phenotype of cancer cells will provide valuable insights for the design and optimization of adjuvant-based chemotherapy.

Supplementary Information The online version contains supplementary material available at https://doi.org/10.1007/s00018-025-05731-8.

Acknowledgements We sincerely appreciate Dr. Qi-En Wang for generously providing the ovarian cancer cell lines. We also extend our gratitude to Ms. Ruby Banerjee for her valuable assistance in acquiring confocal images for this study.

Author contributions Bilash Chatterjee, Mrinmoy Sarkar, and Amit Kumar Srivastava wrote the manuscript. The experiments were performed by Bilash Chatterjee, Mrinmoy Sarkar, Debanjana Ghosh, Sangita Mishra, Subhankar Bose, and Maqsood Ahamad Khan. Visualization, investigation, and data analysis were done by Bilash Chatterjee, Amit Kumar Srivastava, and Mrinmoy Sarkar. Project administration, fund acquisition, and supervision were carried out by Amit Kumar Srivastava. The manuscript was reviewed and edited by Senthil Kumar Ganesan, Mrinmoy Sarkar, Nabanita Chatterjee, and Amit Kumar Srivastava.

Funding This work is supported by internal funding of CSIR-Indian Institute of Chemical Biology (Project no.- OLP-121, Recipient – Dr. Amit Kumar Srivastava).

Data availability The authors confirm that all the raw data files, supporting the findings of this study, are available with the corresponding author and can be obtained upon reasonable request.

Declarations

Ethics approval and consent to participate Human patient samples were obtained from the Chittaranjan National Cancer Institute (human ethics approval-CNCI-IEC-40104). Written consent was obtained from the patients. Animal studies were performed in accordance with institutional animal ethics approval No. IICB/AEC/Meeting/Sep/2023/1. The study was performed in line with the principles of the Declaration of Helsinki.

Competing interest The authors declare that they have no known competing financial and non-financial interests or personal relationships that could have appeared to influence the work reported in this paper.

References

1. Steinhart B, Jordan KR, Bapat J, Post MD, Brubaker LW, Bitler BG, Wrobel J (2021) The spatial context of tumor-infiltrating immune cells associates with improved ovarian cancer survival. Mol Cancer Res 19(12):1973–1979
2. Kumari N, Choi SH (2022) Tumor-associated macrophages in cancer: recent advancements in cancer nanoimmunotherapies. J Exp Clin Cancer Res 41:68
3. Shao S, Miao H, Ma W (2023) Unraveling the enigma of tumor-associated macrophages: challenges, innovations, and the path to therapeutic breakthroughs. Front Immunol 14:1295684
4. Horst EN, Bregenzer ME, Mehta P, Snyder CS, Repetto T, Yang-Hartwich Y, Mehta G (2021) Personalized models of heterogeneous 3D epithelial tumor microenvironments: ovarian cancer as a model. Acta Biomater 132:401–420
5. Motohara T, Katabuchi H (2019) Ovarian cancer stemness: biological and clinical implications for metastasis and chemotherapy resistance. Cancers 11:907
6. Seno M (2025) A landscape of cancer initiation and cancer stem cells. Cancers 17:203
7. El-Tanani M, Rabbani SA, Wali AF, Satyam SM, El-Tanani Y, Aljabali AAA (2025) Deciphering the role of cancer stem cells: drivers of tumor evolution. Ther Resist Precis Med Strateg Cancers 17:382
8. Castells M, Thibault B, Delord J, Couderc B (2012) Implication of tumor microenvironment in chemoresistance: tumor-associated stromal cells protect tumor cells from cell death. Int J Mol Sci 13:9545–9571
9. Pokhriyal R, Hariprasad R, Kumar L, Hariprasad G (2019) Chemotherapy resistance in advanced ovarian cancer patients. Biomark Cancer 11:1–19
10. Varas-Godoy M, Rice G, Illanes SE (2017) The crosstalk between ovarian cancer stem cell niche and the tumor microenvironment. Stem Cells Int 2017:5263974. https://doi.org/10.1155/2017/5263974
11. Chen P, Hsu WH, Han J, Xia Y, DePinho RA (2021) Cancer stemness meets immunity: from mechanism to therapy. Cell Rep 34(1):108597. https://doi.org/10.1016/j.celrep.2020.108597
12. Duan M, Ulibarri J, Liu KJ, Mao P (2020) Role of nucleotide excision repair in cisplatin resistance. Int J Mol Sci 21:9248
13. Anand J, Chiou L, Sciandra C, Zhang X, Hong J, Wu D, Zhou P, Vaziri C (2023) Roles of trans-lesion synthesis TLS DNA polymerases in tumorigenesis and cancer therapy. NAR Cancer 5:1
14. Basak U, Sarkar T, Mukherjee S, Chakraborty S, Dutta A, Dutta S, Nayak D, Kaushik S, Das T, Sa G (2023) Tumor-associated macrophages: an effective player of the tumor microenvironment. Front Immunol 14:1295257. https://doi.org/10.3389/fimmu.2023.1295257
15. Xu J, Fang Y, Chen K, Li S, Tang S, Ren Y, Cen Y, Fei W, Zhang B, Shen Y, Lu W (2022) Single-cell RNA sequencing reveals the tissue architecture in human high-grade serous ovarian cancer. Clin Cancer Res 28:3590–3602
16. Guillaume L (2008) Fast unfolding of communities in large networks. J Stat Mech: Theory Exp 10:P1008. https://doi.org/10.1088/1742-5468/2008/10/P10008
17. Thul PJ, Lindskog C (2018) The human protein atlas: a spatial map of the human proteome. Protein Sci 27(1):233–244
18. Zhou Y, Zhou B, Pache L, Chang M, Khodabakhshi AH, Tanaseichuk O, Benner C, Chanda SK (2019) Metascape provides a biologist-oriented resource for the analysis of systems-level datasets. Nat Commun 10(1):1523
19. Farley DW, Donaldson SL, Comes O, Zuberi K, Badrawi R, Chao P, Franz M, Grouios C, Kazi F, Lopes CT, Maitland A, Mostafavi S, Montojo J, Shao Q, Wright G, Bader GD, Morris Q (2010) The GeneMANIA prediction server: biological network integration for gene prioritization and predicting gene function. Nucleic Acids Res. 38(Web Server issue):W214-20
20. Lu X, Bocangel D, Nannenga B, Yamaguchi H, Appella E, Donehower LA (2004) The p53-induced oncogenic phosphatase PPM1D interacts with uracil DNA glycosylase and suppresses base excision repair. Mol Cell 15:621–634
21. Eslami A, Lujan J (2010) Western Blotting: Sample Preparation to Detection. J Vis Exp 44:e2359. https://doi.org/10.3791/2359
22. Wani TH, Chakrabarty A, Shibata N, Yamazaki H, Guengerich FP, Chowdhury G (2017) The dihydroxy metabolite of the teratogen thalidomide causes oxidative DNA damage. Chem Res Toxicol 30:1622–1628
23. Güç E, Brownlie D, Rodriguez-Tirado C, Kitamura T, Pollard JW (2020) Generation of mouse bone marrow-derived macrophages using tumor coculture assays to mimic the tumor microenvironment. In: Methods in enzymology, vol 632. Academic Press, pp 91–111. https://doi.org/10.1016/bs.mie.2019.11.014
24. Bose S, Saha P, Alam MT, Chatterjee B, Sarkar M, Dixit AK, Kumar D, Pathak RK, Tripathi PP, Srivastava AK (2025) Inhibition of DNA polymerase eta-mediated translesion DNA synthesis with small molecule sensitises ovarian cancer stem-like cells to chemotherapy. Br J Pharmacol 1–18. https://doi.org/10.1111/bph.70037
25. Makridakis NM, Reichardt JKV (2012) Translesion DNA polymerases and cancer. Front Genet 3:174
26. Shilkin ES, Boldinova EO, Stolyarenko AD, Goncharova RI, Chuprov- Netochin RN, Khairullin RF, Smal MP, Makarova MV (2020) Translesion DNA synthesis and carcinogenesis. Biochem Mosc 85(4):425–435
27. Bartha A, Gyorffy B (2021) TNMplot.com: a web tool for the comparison of gene expression in normal, tumor, and metastatic tissues. Int J Mol Sci 22(5):2622
28. Tang Z, Kang B, Li C, Chen T, Zhang Z (2019) GEPIA2: an enhanced web server for large-scale expression profiling and interactive analysis. Nucleic Acids Res 47(W1):W556–W560
29. Barnes RP, Tsao W, Moldovan G, Eckert KA (2018) DNA polymerase eta prevents tumor cell-cycle arrest and cell death during recovery from replication stress. Cancer Res 78(23):6549–6560

30. Wiechert A, Saygin C, Thiagarajan PS, Rao VS, Hale JS, Gupta N, Hitomi M, Nagaraj AB, DiFeo A, Lathia JD, Reizes O (2016) Cisplatin induces stemness in ovarian cancer. Oncotarget 7:21
31. Wang Q, Han C, Zhang B, Sabapathy K, Wani AA (2012) Nucleotide excision repair factor XPC enhances DNA damage-induced apoptosis by downregulating the antiapoptotic short isoform of caspase-2. Cancer Res 72(3):1
32. Li N, Bai X, Cai S, Banerjee A, Yang Y, Ge Q, Wang L, Wang Q (2023) XPC suppresses cancer stem cells by inhibiting STAT1-mediated expression of SOX2 in NSCLC. Cancer Res 83(7_Supplement):2447
33. Wu Y, Cheng Y, Chang JT, Wu T, Chen C, Lee H (2007) Reduced XPC messenger RNA level may predict a poor outcome of patients with non-small cell lung cancer. Cancer 110:215–223
34. Bhaskara S (2015) Histone deacetylases 1 and 2 regulate DNA replication and DNA repair: potential targets for genome stability-mechanism-based therapeutics for a subset of cancers. Cell Cycle 14(12):1779–1785
35. Kusakabe M, Kakumu E, Kurihara F, Tsuchida K, Maeda T, Tada H, Kusao K, Kato A, Yasuda T, Matsuda T, Nakao M, Yokoi M, Sakai W, Sugasawa K (2022) Histone deacetylation regulates nucleotide excision repair through an interaction with the XPC protein. iScience 25:104040
36. Melis JPM, Luijten M, Mullenders LHF, van Steeg H (2011) The role of XPC: Implications in cancer and oxidative DNA damage. Mutat Res 728(3):107–117
37. Yue J, López JM (2020) Understanding MAPK signaling pathways in apoptosis. Int J Mol Sci 21:2346
38. Lin YW, Chuang SM, Yang JL (2003) Persistent activation of ERK1/2 by lead acetate increases nucleotide excision repair synthesis and confers anti-cytotoxicity and anti-mutagenicity. Carcinogenesis 24(1):53–61
39. Larionova I, Tuguzbaeva G, Ponomaryova A, Stakheyeva M, Cherdyntseva N, Pavlov V, Choinzonov E, Kzhyshkowska J (2020) Tumor-associated macrophages in human breast, colorectal, lung, ovarian and prostate cancers. Front Oncol 10:566511
40. Robinson A, Han CZ, Glass CK, Pollard JW (2021) Monocyte regulation in homeostasis and malignancy. Trends Immunol 42:2
41. Sakthivel KM, Hariharan S (2017) Regulatory players of DNA damage repair mechanisms: role in cancer chemoresistance. Biomed Pharmacother 93:1238–1245
42. Xia Y, Shen S, Verma IM (2014) NF-κB, an active player in human cancers. Cancer Immunol Res 2(9):823–830
43. Janssens S, Tschopp J (2006) Signals from within: the DNA-damage-induced NF-κB response. Cell Death Differ 13:773–784
44. Yousef BA, Hassan HM, Zhang L, Jiang ZZ (2018) Pristimerin exhibits *in vitro* and *in vivo* anticancer activities through inhibition of nuclear factor-κB signaling pathway in colorectal cancer cells. Phytomedicine 40:140–147
45. Zhang Y, Wang J, Hui B, Sun W, Li B, Shi F, Che S, Chai L, Song L (2019) Pristimerin enhances the effect of cisplatin by inhibiting the miR-23a/Akt/GSK3β signaling pathway and suppressing autophagy in lung cancer cells. Int J Mol Med 43:1382–1394
46. Li T, Fu J, Zeng Z, Cohen D, Li J, Chen Q, Li B, Liu XS (2020) TIMER2.0 for analysis of tumor-infiltrating immune cells. Nucleic Acids Res. 48(W1):W509–W514
47. Bent EH, Millán-Barea LR, Zhuang I, Goulet DR, Fröse J, Hemann MT (2021) Microenvironmental IL-6 inhibits anticancer immune responses generated by cytotoxic chemotherapy. Nat Commun 12:6218
48. Radharani NNV, Yadav AS, Nimma R, Kumar TVS, Bulbule A, Chanukuppa V, Kumar D, Patnaik S, Rapole S, Kundu GC (2022) Tumor-associated macrophage derived IL-6 enriches cancer stem cell population and promotes breast tumor progression via Stat-3 pathway. Cancer Cell Int 22:122
49. Bois H, Heim TA, Lund AW (2021) Tumor-draining lymph nodes: At the crossroads of metastasis and immunity. Sci Immunol 6:eabg3551
50. Peng JM, Su YL (2023) Lymph node metastasis and tumor-educated immune tolerance: Potential therapeutic targets against distant metastasis. Biochem Pharmacol 215:115731
51. Delclaux I, Ventre KS, Jones D, Lund AW (2024) The tumor-draining lymph node as a reservoir for systemic immune surveillance. Trends in Cancer 10:1
52. Li L, Guan Y, Chen X, Yang J, Cheng Y (2021) DNA repair pathways in cancer therapy and resistance. Front Pharmacol 11:629266
53. Groelly FJ, Fawkes M, Dagg RA, Blackford AN, Tarsounas M (2023) Targeting DNA damage response pathways in cancer. Nat Rev Cancer 23:78–94
54. Zhou H, Zhang JG, Zhang X, Li Q (2021) Targeting cancer stem cells for reversing therapy resistance: mechanism, signaling, and prospective agents. Signal Transduct Target Ther 6:62
55. Fu R, Zhao B, Chen M, Fu X, Zhang Q, Cui Y, Hu X, Zhou W (2024) Moving beyond cisplatin resistance: mechanisms, challenges, and prospects for overcoming recurrence in clinical cancer therapy. Med Oncol 41:9
56. Kouba S, Hague F, Ahidouch A, Ouadid-Ahidouch H (2022) Crosstalk between Ca2+ signaling and cancer stemness: the link to cisplatin resistance. Int J Mol Sci 23:10687
57. Ranasinghe R, Mathai ML, Zulli A (2022) Cisplatin for cancer therapy and overcoming chemoresistance. Heliyon 8:e10608
58. Vaziri C, Rogozin IB, Gu Q, Wu D, Day TA (2021) Unraveling roles of error-prone DNA polymerases in shaping cancer genomes. Oncogene 40:6549–6565
59. Acklin S, Xia F (1975) The role of nucleotide excision repair in cisplatin-induced peripheral neuropathy: mechanism, prevention, and treatment. Int J Mol Sci 2021:22
60. Marteijn J, Lans H, Vermeulen W, Hoeijmakers JHJ (2014) Understanding nucleotide excision repair and its roles in cancer and ageing. Nat Rev Mol Cell Biol 15:465–481. https://doi.org/10.1038/nrm3822
61. Nejad EB, Kleinovink JW, Labrie C, van Elsas MJ, Mittrücker HW, Franken KLMC, Heink S, Korn T, Arens R, van Hall T, van der Burg SH (2021) IL-6 signaling in macrophages is required for immunotherapy- driven regression of tumors. J Immunother Cancer 9:e002460